Author Manuscript

Author Manuscript

Author Manuscript

Author Manuscript

HHS Public Access

Author manuscript

Adv Funct Mater. Author manuscript; available in PMC 2019 May 01.

Published in final edited form as:

Adv Funct Mater. 2018 May ; 28(20): . doi:10.1002/adfm.201707107.

Functionally Graded, Bone- and Tendon-Like Polyurethane for Rotator Cuff Repair

Prof. Dai Fei Elmer Ker,
Department of Orthopaedic Surgery Stanford University 300 Pasteur Drive, Stanford, CA 94305, USA

Institute for Tissue Engineering and Regenerative Medicine The Chinese University of Hong Kong New Territories, Hong Kong SAR

School of Biomedical Sciences Faculty of Medicine The Chinese University of Hong Kong New Territories, Hong Kong SAR

Prof. Dan Wang,
Department of Orthopaedic Surgery Stanford University 300 Pasteur Drive, Stanford, CA 94305, USA

Institute for Tissue Engineering and Regenerative Medicine The Chinese University of Hong Kong New Territories, Hong Kong SAR

School of Biomedical Sciences Faculty of Medicine The Chinese University of Hong Kong New Territories, Hong Kong SARDepartment of Stomatology Tenth People's Hospital of Tongji University Shanghai 200072, China

Anthony William Behn,
Department of Orthopaedic Surgery Stanford University 300 Pasteur Drive, Stanford, CA 94305, USA

Evelyna Tsi Hsin Wang,
Department of Material Science and Engineering Stanford University 496 Lomita Mall, Stanford, CA 94305, USA

Dr. Xu Zhang,
Institute for Tissue Engineering and Regenerative Medicine The Chinese University of Hong Kong New Territories, Hong Kong SAR

School of Biomedical Sciences Faculty of Medicine The Chinese University of Hong Kong New Territories, Hong Kong SAR

Benjamin Yamin Zhou,

D.F.E.K. and D.W. contributed equally to this work.

The ORCID identification number(s) for the author(s) of this article can be found under https://doi.org/10.1002/adfm.201707107.

Supporting Information

Supporting Information is available from the Wiley Online Library or from the author.

Conflict of Interest

The authors declare no conflict of interest.

Author Manuscript Author Manuscript Author Manuscript Author Manuscript

Department of Mathematics Stanford University Building 380, Sloan Mathematical Center, Stanford, CA 94305, USA

Dr. Ángel Enrique Mercado-Pagán,
Department of Orthopaedic Surgery Stanford University 300 Pasteur Drive, Stanford, CA 94305, USA

Dr. Sungwoo Kim,
Department of Orthopaedic Surgery Stanford University 300 Pasteur Drive, Stanford, CA 94305, USA

Dr. John Kleimeyer,
Department of Orthopaedic Surgery Stanford University 300 Pasteur Drive, Stanford, CA 94305, USA

Prof. Burhan Gharaibeh,
Department of Biological Sciences University of Pittsburgh 4249 Fifth Avenue, Pittsburgh, PA 15260, USA

Engineering Research Accelerator Carnegie Mellon University 5000 Forbes Avenue, Pittsburgh, PA 15213, USA

Dr. Yaser Shanjani,
Department of Orthopaedic Surgery Stanford University 300 Pasteur Drive, Stanford, CA 94305, USA

Prof. Drew Nelson,
Department of Mechanical Engineering Stanford University 440 Escondido Mall, Stanford, CA 94305, USA

Prof. Marc Safran,
Department of Orthopaedic Surgery Stanford University 300 Pasteur Drive, Stanford, CA 94305, USA

Prof. Emilie Cheung,
Department of Orthopaedic Surgery Stanford University 300 Pasteur Drive, Stanford, CA 94305, USA

Prof. Phil Campbell, and
Engineering Research Accelerator Carnegie Mellon University 5000 Forbes Avenue, Pittsburgh, PA 15213, USA

Department of Biomedical Engineering Carnegie Mellon University 5000 Forbes Avenue, Pittsburgh, PA 15213, USA

Prof. Yunzhi Peter Yang
Department of Orthopaedic Surgery Stanford University 300 Pasteur Drive, Stanford, CA 94305, USA

Department of Material Science and Engineering Stanford University 496 Lomita Mall, Stanford, CA 94305, USADepartment of Bioengineering Stanford University 443 Via Ortega, Stanford, CA 94305, USA

Author Manuscript Author Manuscript Author Manuscript Author Manuscript

Abstract

Critical considerations in engineering biomaterials for rotator cuff repair include bone-tendon-like mechanical properties to support physiological loading and biophysicochemical attributes that stabilize the repair site over the long-term. In this study, UV-crosslinkable polyurethane based on quadrol (Q), hexamethylene diisocyante (H), and methacrylic anhydride (M; QHM polymers), which are free of solvent, catalyst, and photoinitiator, is developed. Mechanical characterization studies demonstrate that QHM polymers possesses phototunable bone- and tendon-like tensile and compressive properties (12–74 MPa tensile strength, 0.6–2.7 GPa tensile modulus, 58–121 MPa compressive strength, and 1.5–3.0 GPa compressive modulus), including the capability to withstand 10 000 cycles of physiological tensile loading and reduce stress concentrations via stiffness gradients. Biophysicochemical studies demonstrate that QHM polymers have clinically favorable attributes vital to rotator cuff repair stability, including slow degradation profiles (5–30% mass loss after 8 weeks) with little-to-no cytotoxicity in vitro, exceptional suture retention ex vivo (2.79–3.56-fold less suture migration relative to a clinically available graft), and competent tensile properties (similar ultimate load but higher normalized tensile stiffness relative to a clinically available graft) as well as good biocompatibility for augmenting rat supraspinatus tendon repair in vivo. This work demonstrates functionally graded, bone-tendon-like biomaterials for interfacial tissue engineering.

Keywords

biomedical applications; biomimetics; polymeric materials; rotator cuff repair; tissue engineering

1. Introduction

The native bone-tendon interface is highly anisotropic, consisting of a compositionally- and mechanically graded structure with bone- and tendon-like properties. Within this functionally graded structure, multiple musculoskeletal cells, including osteoblasts and tenocytes, secrete specialized extracellular matrices that fulfill the bone-tendon interface's biomechanically demanding role of simultaneously attaching compliant tendon to stiff bone while reducing stress concentrations during musculoskeletal movement.[1,2] Upon injury, however, the bone-tendon interface often heals incompletely, resulting in disorganized and biomechanically inferior scar tissue[3,4] prone to retear. Rotator cuff injuries are typically repaired by affixing suture anchors to humeral bone followed by suture-mediated repair to reestablish a contiguous bone-tendon unit.[5] However, even with surgery, repaired rotator cuff tissues still experience extremely variable and high retear rates ranging from 22%[6] to 91%,[7] and in severe cases where massive tears are present, the damage is deemed irreparable.[5] Although natural and synthetic grafts are clinically available, they reportedly have poor clinical outcomes.[8,9] While the reasons for their lack of efficacy vary, materials that better mimic native bone-tendon biomechanical properties[1,2,10] and possess biophysicochemical attributes that enhance repair stability are expected to reduce retear rates and improve long-term clinical outcomes.

In order to restore biomechanical function to injured rotator cuff tissues, it is vital for grafts to approximate the mechanical properties of bone-tendon tissues. This is because grafts with

Author Manuscript Author Manuscript Author Manuscript Author Manuscript

native tissue-like properties would permit shoulder movement at preinjury levels while minimizing material failure. Clinically available grafts, which are marketed as tendon substitutes, possess tensile strengths (11.9–32.7 MPa)[11] that span or exceed human tendon tissue, however, their tensile moduli (14–71 MPa)[11] are ≈3–42 times lower than native supraspinatus tendon (0.2–0.6 GPa),[12] which is the most frequently injured tendon in rotator cuff injuries.[5,12] In addition, clinically available grafts at this time are not mechanically tunable[9,11,13–17] and lack the capability to reduce stress concentrations via mechanical-gradation. Within this context, prior research has adopted nongraded and graded approaches toward developing improved tendon substitutes or novel bone-tendon grafts, respectively. Promising tendon substitutes include anisotropically aligned collagen biotextiles,[18,19] layered poly(L-lactic acid) scaffolds,[20,21] electrospun nanofibers with crimped morphology,[22] collagen scaffolds crosslinked via hypoxia and lysyl oxidase,[23] woven poly(L-lactic acid) scaffolds[24] and tyramine substituted-hyaluronan enriched fascia extracellular matrix[25] while pioneering work on mechanically graded grafts include multiphased scaffolds,[26–28] anisotropic collagen-GAG scaffolds,[29–31] “aligned-to-random” nanofiber scaffolds,[32,33] poly(lactic-*co*-glycolic acid) or polycaprolactone nanofibers with mineral gradients,[34,35] and bone-tendon allografts.[36] However, biomaterials that better approximate the stiffness gradient of bone-tendon tissues are needed. For example, a gradient of calcium phosphate was applied across electrospun nanofibers to mimic the transitional nature of the bone-tendon interface,[34,35] but the tensile moduli only ranged between 40–120 MPa.[34] Although such work demonstrates substantial advancement in mechanically graded graft fabrication, these values fall short of physiologically relevant tendon and bone moduli by 5–15 and 92–242 folds, respectively.[12,37–39] The importance of possessing physiological mechanical properties is underscored in studies[40,41] that demonstrate suboptimal tendon stiffness negatively impacts musculoskeletal efficiency and performance. Thus, further improvements are essential toward achieving grafts with bone-tendon-like mechanical properties.

In order to facilitate long-term repair stability, it is also vital for grafts to possess biophysicochemical characteristics beneficial for clinical implementation. These include but are not limited to good physical integrity (slow degradation), secure physical attachment (good suture-retention) and graft competence (adequate biocompatibility and restoration of shoulder function after repair). This is because grafts that degrade slowly, resist tears and exhibit an optimal tissue response while sustaining shoulder function will maintain sufficient repair integrity to allow a patient to resume daily activities while facilitating bone-tendon healing. The importance of slow degradation was demonstrated when rapidly degrading rotator cuff patches were used to treat massive rotator cuff tears.[17] These rotator cuff patches degraded completely within 3–6 months post-surgery and were associated with failed repairs as well as other complications.[17] Similar scenarios have been observed for rapidly degrading suture anchors that resulted in clinical complications, such as loose suture bodies,[42] or were suspected of causing suture anchor migration.[43] Also, slow degradation is desirable since it minimizes toxicity effects and adverse tissue responses. For example, osteolysis, although uncommon, has been observed more frequently in fast-degrading polyglycolide-based suture anchors[44] compared to slow-degrading poly-L-lactic acid-based suture anchors.[45] The importance of providing secure musculoskeletal attachment has been

Author Manuscript Author Manuscript Author Manuscript Author Manuscript

demonstrated by ex vivo biomechanical analysis of surgically repaired rotator cuff tears.[46,47] Although the initial strength of rotator cuff repair can be improved by various repair techniques, its integrity can still be compromised by gap formation between tendon and bone even at low physiologic loads.[46] Such repairs may subsequently fail by tendon pull-through of the suture.[47] The importance of graft competence was demonstrated when xenografts based on the small intestinal mucosa of pigs were used to treat rotator cuff tears.[9] No clinically recognizable benefit was found as these rotator cuff patches presented similar retear rates but with significantly less shoulder strength, lower range of motion and slower pain resolution compared to the traditional repair group.[9] Also, poor graft biocompatibility resulted in severe inflammatory reactions for several patients and additional surgical treatment became necessary.[9] Thus, a graft that possesses long-term physical integrity, security of tendon-to-bone attachment and competence in restoring shoulder function as well as biocompatibility is highly desirable.

To address the afore-mentioned challenges in rotator cuff repair, we developed a slow-degrading, photo-tunable polymer with robust bone- and tendon-like mechanical properties. To achieve this, a combination of chemical-crosslinking, photo-crosslinking, and heat-curing was utilized to fabricate highly crosslinked, photo-tunable polyurethane networks with slow hydrolyzable bonds. Here, quadrol (Q), hexamethylene diisocyanate (H) and methacrylic anhydride (M) were used to develop solvent-, catalyst- and photoinitiator-free, UV-crosslinkable polyurethane (QHM polymers) that possess robust, photo-tunable bone- and tendon-like mechanical properties, including the ability to sustain at least 10,000 cycles of physiologic loading as well as reduce stress concentrations via stiffness gradation. These QHM polymers also exhibited slow degradation profiles, minimal cytotoxicity, exceptional suture retention properties, and competent biomechanical as well as biocompatible attributes in a rat supraspinatus tendon injury model.

2. Results

2.1. Synthesis and Physicochemical Characterization of UV-Crosslinkable QHM Polymers

The fabrication of QHM polymers was monitored by ^{1}H-NMR and Fourier transformed infrared spectroscopy (FTIR)- attenuated total reflection (ATR) spectroscopy (Figure 1). QHM polymers were synthesized from Q, H, and M (Figure 1a). ^{1}H-NMR spectra of Q/H/M showed characteristic peaks observed in individual ^{1}H-NMR spectra of Q, H, and M (Figure 1b; Table S1, Supporting Information).[48,49] FTIR-ATR spectra of Q/H, Q/M, and H/M prepolymers indicated chemical reactions between Q and H (Figure S1a, Supporting Information) as well as Q and M (Figure S1b, Supporting Information) but not between H and M (Figure S1c, Supporting Information). FTIR-ATR spectra of Q/H/M prepolymer indicated reactions between the hydroxyl groups of Q and isocyanate groups of H to form carbamate groups as well as the hydroxyl groups of Q and the anhydride carbonyl groups of M to form ester groups (Figure 1c; Table S2, Supporting Information).[48–50] ^{1}H-NMR spectra of QHM polymers indicated increased crosslinking with longer UV exposure (Figure S1d, Supporting Information). Physiologically relevant, microscale mechanical-gradation was exemplified by synthesizing alternating regions of 0 and 300 s UV QHM polymers (Figure S2, Supporting Information). Together, these data demonstrated the presence of

Author Manuscript Author Manuscript Author Manuscript Author Manuscript

polyurethane carbamate groups, methacrylation, and UV-crosslinking during polymer fabrication.

2.2. Effect of UV Exposure on the Mechanical Properties of QHM Polymers

The mechanical properties of QHM polymers were determined by tensile, compressive, creep, and cyclic testing (Figures 2 and 3). Pilot studies showed increased strength and elastic moduli with heat-curing (data not shown). Thus, heat-cured QHM polymers were used for the remainder of this study.

QHM polymers exhibited photo-tunable tensile properties. The tensile strength and moduli of QHM polymers increased with longer UV exposure, ranging from 12 to 74 MPa and 0.6 to 2.7 GPa, respectively, whereas those of QH polymer controls were largely unaltered (Figure 2a; Tables S3–S5, Supporting Information). Tensile strain at yield or failure of QHM polymers initially decreased with short (<90 s) UV exposure and remained unchanged thereafter whereas QH polymer controls were largely unaltered (Figure 2a; Tables S3 and S6, Supporting Information). QHM polymers exhibited phototunable compressive properties. The compressive strength and moduli of QHM polymers increased with longer UV exposure, ranging from 58 to 121 MPa and 1.5 to 3.0 GPa, respectively, whereas those of QH polymer controls were largely unaltered (Figure 2b; Table S7–S9, Supporting Information). Strain at maximum compressive stress of QHM and QH polymers was largely unaltered with UV exposure (Figure 2b; Tables S7 and S10, Supporting Information). Differential scanning calorimetry (DSC) indicated that at body temperature (37 °C), 0 s UV and 90 s UV QHM polymers exhibit compliance whereas 180 s UV and 300 s UV QHM polymers remain stiff (Figure S3, Supporting Information).

Tensile creep and cyclic testing determined the robustness of 0 s UV QHM polymer as a tendon substitute. In static creep tests, 0 s UV QHM polymers exhibited 1.7% strain following a 30 min hold at 3 MPa tensile stress and recovered 0.8% strain following a 10 min recovery period (Figure 3a). Creep rate was 0.035% per min. In cyclic tensile tests, 0 s UV QHM polymers exhibited 2.4% strain, consistent dynamic (1.5–1.8 GPa), storage (1.5–1.8 GPa), and loss moduli (0.3 GPa) as well as tan δ (0.18–0.20) during 10 000 loading cycles from 0.2 to 3 MPa tensile stress (Figure 3b and data not shown). Specimens reached steady state response after ≈4000 cycles. A single specimen tested for 100 000 loading cycles exhibited 5.7% strain without failure and recovered following unloading (Figure S4, Supporting Information).

Thus, QHM polymers demonstrated phototunable mechanical properties including increased strength and modulus with longer UV exposure while 0 s UV QHM polymer showed robust fatigue and recovery attributes.

2.3. Effect of Stiffness Gradients on Stress Concentration Reduction in QHM Polymers

The effect of stiffness gradients of QHM polymers on reducing stress concentrations was determined by finite element analysis (FEA) and photoelastic tensile testing (Figures 4 and 5). In FEA (Figure 4a), the greatest stress concentration was observed in steeply graded models at the intersection of the interface and free edge, with high stress levels primarily in the model's stiffer region near the interface and a centrally located stress decrease in the

Author Manuscript Author Manuscript Author Manuscript Author Manuscript

model's compliant region near the interface (Figure 4b). Varying Poisson's ratio yielded similar results, primarily affecting stress magnitude (Figure S5, Supporting Information). In photoelastic tensile testing (Figure 5a; Figure S6, Supporting Information), gradually graded specimens reduced stress concentrations relative to more steeply graded specimens (Figure 5b), corroborating FEA results. Gradually- and steeply graded specimens subjected to tensile testing failed in the bulk material of the weaker top half but not at the interface (data not shown). Thus, gradual-gradation reduced stress concentrations.

2.4. Functionally Graded Biomaterial as a Hybrid Suture Anchor-Tendon Graft

Since the design of functionally graded biomaterials is crucial for seamless integration of stiff bone with compliant tendon,[2] we briefly explored a potential form factor to facilitate clinical translation. The mechanical-gradation of QHM polymers was demonstrated with compliant regions exhibiting larger strain relative to stiffer regions in the presence of mechanical loading (Figure 6a). Also, QHM polymers were fabricated into a functionally graded, hybrid suture anchor-tendon graft that could be sutured as well as anchored to faux bone (Figure 6b).

2.5. Degradation of QHM polymers

To determine the integrity of QHM polymers under simulated body conditions, including chronic wound environments, foreign body reaction to implanted materials and normal physiological conditions, degradation studies were performed. QHM polymer samples were incubated under alkaline (5 N NaOH), acidic (2 N HCl), oxidizing (30% H_2O_2), and aqueous (Hank's buffered salt solution, HBSS) conditions for 8 weeks and their mass (dry weight) was recorded (Figure 6c). Under alkaline, acidic, oxidizing, and aqueous conditions, QHM polymers exhibited little to no mass loss, 5–30% mass loss, 10–30% mass loss, and 5–10% mass loss after 8 weeks, respectively (Figure 6d). QHM polymers exhibited little to no swelling under alkaline and aqueous conditions, whereas swelling ratios between 1.5 and 2.0 were observed under acidic and oxidizing conditions (Figure 6e). C2C12 cells cultured in 8 week HBSS degradation products (diluted 1:9) proliferated similarly to control (Figure 6f; Table S11, Supporting Information) and exhibited myogenic differentiation (Figure 6g), indicating unperturbed cell behavior. Thus, QHM polymers degraded slowly and their degradation products exhibited little to no cytotoxicity.

2.6. Suture retention of 0 s UV QHM polymer

Since rotator cuff repairs frequently fail by tendon pull-through of suture,[47] suture retention studies were performed to assess the ability of tendon-like 0 s UV QHM polymer to sustain surgical repair. 0 s UV QHM polymer exhibited 2.79-fold less suture migration after 500 loading cycles from 0.0 to 7.5 N (Figure 7a; Table S12, Supporting Information; $p = 0.002$) and 3.56-fold less suture migration during pull-to-failure (at 25 N) relative to a clinically available acellular dermal matrix (ADM) (Figure 7b; Table S13, Supporting Information; $p = 0.001$). Thus, 0 s UV QHM polymers demonstrated superior suture retention properties relative to ADM.

Author Manuscript Author Manuscript Author Manuscript Author Manuscript

2.7. Biomechanical and Biocompatible Properties of 0 s UV QHM polymer

To determine the ability of 0 s UV QHM polymer to function as a tendon substitute, rat rotator cuff injury studies were performed. In these studies, rat supraspinatus tendons were transected and repaired with either 0 s UV QHM polymer or ADM (Figure 8). Both 0 s UV QHM polymer and ADM contained growth and differentiation factor-7 (GDF-7), which has been shown to induce ectopic tendon or ligament formation in rats and has shown promise as an adjuvant for rotator cuff repair in clinical studies.[51,52] Rats implanted with either 0 s UV QHM polymer or ADM showed consistent weight gain and did not exhibit adverse clinical signs or mortality, including detrimental reactions such as necrosis and infection around the implants (data not shown). Paired biomechanical testing of supraspinatus muscle-tendon-bone units 8 weeks postsurgery demonstrated that although 0 s UV QHM polymer and ADM exhibited similar ultimate load (Figure 8a; Table S14, Supporting Information; $p = 0.919$), 0 s UV QHM polymer showed increased normalized tensile stiffness (Figure 8b; Table S14, Supporting Information; $p = 0.040$). Histological staining demonstrated the presence of elongated tendon-like cells (hematoxylin and eosin stain) embedded within aligned and wavy collagen fibers (Trichrome stain) adjacent to 0 s UV QHM polymer (Figure 8c). Histological staining also showed high levels of cell infiltration in ADM (Figure 8c). Thus, 0 s UV QHM polymers demonstrated competent biome-chanical and biocompatible properties for augmenting repair of rat supraspinatus tendon.

3. Discussion

Rotator cuff tears are common shoulder injuries with over 200 000 surgeries performed annually in the United States at an estimated cost of USD 3.44 billion.[53] Engineering biomaterials that provide adequate biomechanical function as well as promote better repair stability hold great promise to mitigate this burden. This study developed a solvent-, catalyst- and photoinitiator-free UV-crosslinkable biomaterial (Figure 1) that recapitulated several vital features of bone-tendon tissues, however, to reduce material complexity[2] and facilitate clinical translation, the native bone-tendon interface was not reproduced in its entirety. Major features of our graft addressed here include: (1) robust, phototunable bone- and tendon-like mechanical properties (Figures 2 and 3), including the capability to reduce stress concentrations via stiffness gradients (Figures 4 and 5); and (2) biophysicochemical characteristics favorable for clinical translation, including slow degradation with minimal cytotoxicity (Figure 6), excellent suture retention capabilities (Figure 7), and capability to function as a tendon substitute (Figure 8).

Development of a novel biomaterial with native tissue-like mechanical properties is vital for restoring biomechanical function. Specifically, the human supraspinatus tendon, which is commonly torn in rotator cuff injuries,[5,12] has tensile strength ranging from 4 to 22 MPa[12,37] and a tensile modulus ranging from 0.2 to 0.6 GPa[12,37] while cortical bone has tensile strength ranging from 66.0 to 170.0 MPa,[38,39] a tensile modulus ranging from 11.0 to 29.0 GPa, compressive strength ranging from 167 to 213 MPa and a compressive modulus ranging from 14.7 to 34.3 GPa.[38,39] These properties are important since bone is often subjected to compressive and tensile forces, while tendon and fibrocartilaginous transitional regions experience both tensile and compressive stress particularly at locations they wrap

Author Manuscript Author Manuscript Author Manuscript Author Manuscript

around bony or fibrous pulleys.[54,55] Moreover, tendons that are overly or insufficiently stiff relative to physiological values decrease the efficiency of joint motion.[40,41] QHM polymers exhibited phototunable tensile strength (12–74 MPa) and moduli (0.6–2.7 GPa) that approximated bone and tendon tissues (Figures 2 and 3; Figures S4 and S5, Supporting Information). This represents a marked improvement over clinically available grafts,[11] which are not mechanically tunable, as well as those previously reported in other research efforts,[34] which did not approximate the moduli of mature bone-tendon tissues. Thus, bone- and tendon-like mechanical properties of QHM polymers are expected to sustain physiological loading.

QHM polymers were able to approximate the mechanical properties of bone and tendon tissues due to its unique fabrication approach. In general, highly crosslinked polymers possess increased molecular weights and mechanical properties.[56] Q is a tetrafunctional monomer with hydroxyl groups that react with the isocyanate and anhydride groups of H and M, respectively, producing a highly crosslinked polyurethane network with high mechanical properties (Figures 1 and 2; Figure S1, Supporting Information). The phototunable capability arises from vinyl methine groups of M that participate in UV-crosslinking. Solvents, catalysts or photoinitiators were not required as monomer(s) were miscible, able to pseudocatalyze polyurethane reactions[57] and self-initiate photopolymerization,[58] respectively. By selecting a desired ratio of Q, H, and M monomers as well as varying UV exposure, the desired level of chemical- and photo-crosslinking within QHM polymer chains were attained. Post-processing of QHM polymers by heat-curing likely promoted physical chain entanglements that further contributed to increased mechanical properties (data not shown). Ultimately, these two modes of crosslinking together with heat-curing allowed QHM polymers to achieve high, photo-tunable mechanical properties.

In addition to bone- and tendon-like strength and moduli, a bone-tendon biomaterial that exhibits robustness and reduces stress concentrations will be advantageous for restoring biomechanical function and minimizing material failure. These properties are important since bone and tendon tissues can typically withstand numerous and challenging loading regimens without failure.[39,59,60] In particular, the functional attachment of bone to tendon requires tissue architectures that mitigate increased stress concentrations due to their mechanical mismatch. In healthy, native attachment sites, this is accomplished, in part, by gradations in mineral content and collagen fiber orientation along the bone-tendon interface to create a resilient and functionally graded interface.[1,55,61–63] Indeed, bone-tendon repairs that fail to restore native tissue mechanical properties show little to no regeneration of its graded fibrocartilaginous transition.[1–4] In cyclic tensile tests, 0 s UV QHM polymer demonstrated robust, tensile properties by withstanding at least 10 000 cycles of physiologic loading (Figure 3; Figure S4, Supporting Information). In addition, the dynamic modulus (1.5–1.8 GPa) and tan δ (0.18–0.20) of 0 s UV QHM polymer (Figure 3; Figure S4, Supporting Information) approximated the dynamic modulus of sheep plantaris tendon (1.37–1.99 GPa)[64] as well as the tan δ for rabbit Achilles tendon (0.108–0.180).[65] DSC studies showed that 0–90 and 180–300 s of UV light exposure resulted in QHM polymers with glass transition temperatures below and above 37 °C, respectively (Figure S3, Supporting Information). Given that polymers exhibit compliance and stiffness at

Author Manuscript Author Manuscript Author Manuscript Author Manuscript

temperatures above and below their glass transition temperatures, respectively,[56] mechanical-gradation of QHM polymers is expected to approximate the compliant-to-stiff transition of a contiguous bone-tendon unit (Figure 6). Since QHM polymers are phototunable and current photolithography techniques can achieve nanometer-scale resolutions, such stiffness gradients can be fabricated at physiologically relevant lengths (Figure S2, Supporting Information). In addition, FEA and photoelastic tensile testing of QHM polymers showed that gradual stiffness gradients reduced stress concentrations (Figures 4 and 5; Figures S5 and S6, Supporting Information). Thus, the robustness and ability of QHM polymers to reduce stress concentrations via gradual gradation is expected to minimize material failure during physiological loading.

In addition to engineering robust, native tissue-like mechanical properties that reduce stress concentrations via stiffness gradients, clinical translation would benefit from a bone-tendon biomaterial that maintains repair stability in synchronicity with healing duration. This includes slow and tunable degradation properties, the capacity for secure suture attachment and adequate restoration of shoulder function following repair. To facilitate clinical translation, QHM polymers were fabricated into a mechanically graded, continuous bone-tendon graft (Figure 6). This design concurs with calls for multiphasic or gradient-based scaffolds that strategically mimic complex musculoskeletal tissue interfaces[2] and was based, in part, on our FEA and photoelastic studies which showed that gradual stiffness gradients reduced stress concentrations (Figures 4 and 5; Figures S5 and S6, Supporting Information). Although suture anchor-mediated repair facilitates the reapproximation of torn tendon back to its original anatomical location,[5] the continuity of the bone-tendon unit is disrupted and potential failure modes are introduced, including suture breakage at the eyelet[66] and loosening of suture eyelets as a result of degradation.[67] These failure modes are eliminated by fashioning QHM polymers into a continuous compliant-to-stiff form factor. While there are numerous design permutations for a continuous bone-tendon graft, this particular form factor was inspired by combining two existing medical devices used in rotator cuff repair—a suture anchor and a tendon graft. This design will be familiar to surgeons and may promote end user adoption. This continuous design also innovates upon suture anchors, whose role has not fundamentally changed since their introduction in 1906 as a bone anchoring device,[68] into one that is simultaneously both a bone anchor and tendon graft. However, regardless of form factor or design, further studies are required to determine whether such bone-tendon devices may be used in an interpositional fashion (which only bridges the tear gap) or augmented fashion (which bridges the tear gap as well as overlaps with remaining tendon). Such testing was not feasible within the small confined shoulder space of our rat injury model. To ensure good physical integrity, a bone-tendon biomaterial must exhibit degradation characteristics in synchronicity with the healing duration. Although optimal degradation rates are patient- and injury-dependent, slow degradation rates are ideal[17,42] given the lengthy recovery periods for rotator cuff injuries.[5] Premature degradation would compromise the graft's integrity and mechanical properties to sustain physiological loading[27,42] and has been suggested as a possible reason for the failure of graft-mediated rotator cuff repair.[17] Our degradation studies showed that QHM polymers degraded slowly under aqueous, acidic, alkaline, and oxidizing conditions (Figure 6), which was likely attributed to its high content of slow-to-hydrolyze carbamate groups.

Author Manuscript Author Manuscript Author Manuscript Author Manuscript

[56,57] These conditions were selected to approximate normal physiological conditions, chronic wound healing conditions (where either acidic or alkaline pH persist)[69] as well as foreign body reaction to biomaterials (where reactive oxygen species are generated in a low pH environment by macrophages and foreign body giant cells).[70] Also, in vitro studies indicate that the degradation products of QHM polymers exhibited little to no cytotoxicity (Figure 6). Further studies are required to characterize the degradation of QHM polymers in vivo and determine how loss of physical integrity correlates with important considerations such as biomechanical strength. To ensure secure physical attachment to musculoskeletal tissues, a bone-tendon biomaterial must resist suture tear through since this is a frequently observed mode of failure for rotator cuff repair.[47] In suture retention tests, 0 s UV QHM polymer demonstrated 2.79- and 3.56-fold less suture migration after 500 cycles of loading and during load to failure when compared to a popular, clinically available ADM marketed for rotator cuff augmentation (Figure 7). To ensure adequate graft performance, a bone-tendon biomaterial should exhibit good biocompatibility and restore shoulder function following repair. Frequently, this parameter is assessed by histological and biomechanical testing of the repaired bone-tendon unit[71,72] although ambulatory measures such as medial/lateral forces, braking, propulsion, and step width[73] may better approximate clinical measurements of patient outcome.[74] When employed as a tendon substitute to augment repair of rat supraspinatus tendon, 0 s UV QHM polymer demonstrated competent biomechanical properties including similar ultimate load but higher normalized tensile stiffness compared to ADM (Figure 8). Both 0 UV QHM polymer and ADM also contained GDF-7, a tendon-promoting growth factor,[52] to supplement tissue healing. GDF-7 was chosen since subcutaneous implantation of an inert carrier containing this growth factor resulted in ectopic formation of tendon/ligament in rats.[52] Also, there is tremendous clinical interest in using GDF-7 for rotator cuff repair—a randomized, multicenter clinical trial employing this growth factor as an adjuvant therapy showed decreased pain as well as improved shoulder strength and range of motion following surgery.[51] Supplementation of such biological cue(s) aim to reestablish resident musculoskeletal cells to regenerate and maintain native tissue phenotype(s). Prior efforts in this regard included delivering bone- and tendon-promoting growth factors as well as extracellular matrices,[31,52,75–78] using unmodified[78] or genetically engineered stem cells,[79–83] and platelet-rich plasma.[77] Preliminary histological analysis demonstrated the presence of tendon-like tissue (elongated cells with flattened nuclei embedded within aligned and wavy collagen fibers) adjacent to 0 s UV QHM polymer while high levels of cell infiltration were observed in ADM (Figure 8). Exuberant levels of inflammation were not observed, indicating both 0 s UV QHM polymer and ADM were biocompatible. However, further work such as inclusion of grafts without GDF-7 as well as using polarized light microscopy and immunostaining of tendon-specific markers will be required to ascertain the effect of 0 s UV QHM polymer (with or without GDF-7) on tendon healing and regeneration. Understanding this will be crucial in determining whether there is a need to optimize growth factor choice, dose and delivery prior to attempting a larger injury or animal model. Ultimately, QHM polymers possessed biophysicochemical characteristics favorable for repair stability and clinical translation, which are expected to facilitate eventual integration between graft and host tissue.

Author Manuscript Author Manuscript Author Manuscript Author Manuscript

4. Conclusion

In summary, a mechanically graded polyurethane has been developed using a unique approach that achieved bone- and tendon-like mechanical properties and biophysicochemical characteristics favorable for bone-tendon repair.

5. Experimental Section

Material Fabrication

N,*N*,*N*′,*N*′-tetrakis(2-hydroxy-propyl) ethylenediamine (quadrol or Q; Sigma Aldrich, St. Louis, MO), 1,6-diisocyanatohexane (H; Sigma Aldrich, St. Louis, MO), and methacrylic anhydride (MA or M; Sigma Aldrich, St. Louis, MO) were used as received without further purification. Q, H, and M were mixed in a 50 mL conical tube at a molar ratio of 1:1.5:0.5, respectively, prior to vigorous vortexing for 1–2 min. Subsequently, the QHM mixture was degassed in a vacuum desiccating chamber (Bel-Art Products, Wayne, NJ) using a Welch DuoSeal 1405 vacuum pump (Welch-llmvac, Niles, IL) for 0.5–1 min and transferred into the appropriate mold(s). The mold(s) were degassed for an additional 20 to 30 min and placed in a custom-made light cabinet (42 cm × 22 cm × 62 cm) equipped with an OmniCure Series 2000 UV system (Excelitas Technologies Illumination, Fremont, CA) and a collimating adapter (Excelitas Technologies Illumination, Fremont, CA). Irradiance at the emitting end of the 5 mm OmniCure light guide was adjusted to 7 W cm^{-2} using an OmniCure R2000 radiometer (Excelitas Technologies Illumination, Fremont, CA). Molds were positioned 60 cm from the collimating adapter, UV-crosslinked for the indicated durations (0, 90, 180, 300, or 0–300 s; where necessary, aluminum foil was used as a photomask) and placed in a pressure pot chamber (Finish Systems, New Berlin, WI) at 40 psi under nitrogen atmosphere overnight. The following day, QHM polymer samples were released from their molds, sanded using a Ryobi Belt Sander (80–120 grit; Ryobi Limited, Fuchu-Shi, Japan) and heat-cured between 85–100 °C for 5–6 h in a heating oven (Thermo Fisher Scientific, Waltham, MA). Subsequently, QHM polymer samples were washed once in 5 N sodium hydroxide (Ricca Chemical Company, Arlington, TX) for 1 h, washed five times in deionized water and air-dried. Specimen dimensions are described below for each study.

Nuclear Magnetic Resonance Spectroscopy (NMR)

^{1}H-NMR was performed using a Varian Inova 300 instrument (Varian Inc., Palo Alto, CA) at ambient conditions. Samples of QHM prepolymer or UV-crosslinked QHM polymer were dissolved overnight at 4 °C in deuterated chloroform ($CDCl_3$; 99.8% deuterated, Sigma Aldrich, St. Louis, MO) to obtain maximum solubility. Pure $CDCl_3$ was used as an internal standard. NMR spectra prediction was performed with ChemBioDraw Ultra 13.0 software (CambridgeSoft, Waltham, MA). NMR data were analyzed with MestReNova 10.0 NMR software (Mestrelab Research, Escondido, CA).

Fourier Transformed Infrared Spectroscopy

FTIR was performed using a Bruker Vertex 70 spectrometer (Bruker Optics Inc., Billerica, MA) and analyzed with OPUS optical spectroscopy software (Bruker Optics Inc., Billerica,

Author Manuscript Author Manuscript Author Manuscript Author Manuscript

MA). For Q/H prepolymer solutions, Q and H were mixed at a molar ratio of 1:2, respectively. For Q/M prepolymer solutions, Q and M were mixed at a molar ratio of 1:4, respectively. For H/M prepolymer solutions, H and M were mixed at a molar ratio of 1:1, respectively. For QHM prepolymer solutions, Q, H, and M were mixed at a molar ratio of 1:1.5:0.5, respectively. Prepolymer solutions were mixed vigorously for 5–10 min and samples were placed in the holder directly in the IR laser beam. Degassing and longer prepolymer reaction times were not attempted to avoid polymer solidification within the sample holder. All spectra were recorded (40 averaged scans, 800–4000 cm^{-1}) at a resolution of 4 cm^{-1}. Spectra were baseline-corrected and smoothed in the OPUS spectroscopy software.

Mechanical Testing

QHM polymer samples were mechanically tested under dry conditions at room temperature following the guidelines in the American Society for Testing and Materials methods D638-10 (Tensile properties of plastics), D695-10 (Compressive properties of rigid plastics), and D7791-12 (Uniaxial fatigue properties of plastics). Although tendons are predominantly subjected to tensile stress, there are locations where tendons experience compressive stresses, most notably where they wrap around bony or fibrous pulleys and at the bone-tendon interface. Consequently, both tension and compressive tests were performed on the QHM polymer samples. Tensile testing samples were fabricated as dog bone-shaped specimens with an overall length of 115 mm with the narrow region measuring 3 mm (thickness) × 7.5 mm (width) × 33 mm (length). Compression testing samples were fabricated as rectangular specimens measuring 25 mm (height) × 6 mm (width) × 8 mm (length). The average cross-sectional area was determined from three locations along the specimen length using digital calipers (Digimatic IP67 Coolant-Proof Caliper; Mitutoyo American Corporation, Aurora, IL). A Model 5944 test system equipped with a 2 kN load cell (Instron Corp., Norwood, MA) was used for tensile testing whereas an ElectroPuls E10000 test system (Instron Corp., Norwood, MA) was used for compressive, creep and cyclic testing. Compression tests were performed using a 10 kN load cell whereas creep and cyclic tests incorporated a 250 N load cell. Strain was determined using an extensometer (Model: 3442-0064-050-ST, Gauge length: 16.3 mm, Epsilon Technology Corp, Jackson, WY).

For tensile testing, QHM polymer samples were preloaded to 5 N and subsequently uniaxially loaded at a rate of 0.65 mm per second until failure. This displacement rate corresponds to a strain rate of ≈1% strain per second during loading in the initial region of linear response. For QHM polymer samples that did not fail (break) before 50% strain, the extensometer was removed and testing was continued until failure. Tensile strength at yield or break was defined as tensile stress at which QHM polymer samples yielded (slope where the stress–strain curve equals zero) or failed, respectively. Tensile strength at break was reported for samples that did not yield. Tensile modulus was defined as the initial linear slope of the stress–strain curve and calculated from 0% to 1% strain. Tensile strain at yield or break was defined as the strain at which QHM polymer samples yielded or failed, respectively. Tensile strain at break was reported for samples that did not yield. Failure strain

Author Manuscript Author Manuscript Author Manuscript Author Manuscript

for QHM polymer samples that did not break before 50% strain was calculated using the machine readout of grip separation.

For compressive testing, QHM polymer samples were preloaded to 10 N and then uniaxially loaded at a strain rate of 1% s^{-1} until failure. Compressive strength was defined as the maximum compressive stress achieved during the test as QHM polymer samples failed by buckling. Compressive modulus was defined as the initial linear slope of the stress-strain curve and calculated from 1% to 2% strain. Compressive strain at maximum stress was defined as the strain at which maximum compressive stress was achieved during the test.

For static creep tensile testing, QHM polymer samples were loaded in tension to 3 MPa (which was estimated[12,37,84] to be 75% of the maximum stress generated by supraspinatus muscle) for 30 min. Specimens were then rapidly unloaded to 0 MPa and recovery was monitored for 10 min. Static creep was defined as the difference in strain between the initial and final time points during the 30 min hold at 3 MPa. Creep recovery was defined as the difference in strain after the 30 min hold at 3 MPa and the 10 min recovery period at 0 MPa. Creep rate was determined from the linear slope of the strain–time curve between 10 and 30 min during loading at 3 MPa.

For cyclic tensile testing, QHM polymer samples were loaded from 0.2 to 3 MPa for 10 000 cycles at 1 Hz. The lower loading limit of 0.2 MPa was selected as an estimate of the passive tension generated by the supraspinatus muscle.[85] The dynamic, storage and loss modulus as well as tan δ were calculated at various time points during cyclic loading using WaveMatrix software (Instron Corp., Norwood, MA). The dynamic modulus was defined as the ratio of the stress range to strain range of the hysteresis loop for a given loading cycle. The storage modulus was defined as the dynamic modulus multiplied by the cosine of the loss angle. The loss modulus was defined as the dynamic modulus multiplied by the sine of the loss angle. tan δ was defined as the ratio of the loss modulus to the storage modulus. Cyclic creep was defined as the difference in strain at 3 MPa between cycle 10 and cycle 10 000.

Differential Scanning Calorimetry

DSC was performed using a Q100 instrument (TA Instruments, New Castle, DE) under nitrogen atmosphere and analyzed with Universal Analysis software (TA Instruments, New Castle, DE). QHM polymer samples were crushed with a hammer to obtain samples weighing 10–20 mg and sealed in an aluminum pan. QHM polymer samples were subjected to cool– heat–cool–heat treatment over a temperature range of −40 to 100 °C. The first run started from room temperature cooling to −40 °C, holding isothermally for 5 min, followed by heating from −40 to 100 °C and holding isothermally at 100 °C for 5 min. The second run started from 100 °C cooling to −40 °C, holding isothermally for 5 min, followed by heating from −40 to 100 °C. Heating or cooling was performed at a rate of 20 °C min^{-1}. The glass transition temperature (T_g) was measured at the midpoint of the transition process from the second run.

Author Manuscript Author Manuscript Author Manuscript Author Manuscript

Finite Element Analysis

Linear static FEA of a mechanically graded specimen containing a single bonded interface was performed using SolidWorks Simulation (Dassault Systemes, Waltham, MA). While simplistic, a single interface was simulated since gradients can be approximated by a continuous series of discrete intervals. Moreover, this setup facilitated ease of comparison with photoelastic tensile testing. Due to symmetry, a quarter model was developed with similar geometry to QHM polymer samples used for tensile testing. The dimensions were 10 mm (overall length) × 3 mm (half-width) × 1.5 mm (half-thickness). The 10 mm overall length was selected to analyze the loading distribution in the vicinity of the interface. Roller boundary conditions were modeled along the midplanes of the model (right and back faces). An additional roller boundary condition was applied to the bottom face of the model to prevent vertical (γ axis) displacement. A uniform tensile stress (10 MPa) was applied to the model's top face to simulate a physiologically relevant load close to the tensile strength of supraspinatus tendon.[37]

The model mesh was created using second-order tetrahedral elements varying in size from 0.125 mm away from the interface down to 0.005 mm along the periphery of the interface. Due to the stress singularity at the interface, convergence of the model was not reached with further mesh refinement. The elastic moduli and Poisson's ratio were defined using linear elastic isotropic material models. A Poisson's ratio of 0.3 and an elastic modulus of 0.5 GPa were used for the top rectangular cuboid while a Poisson's ratio of 0.3 and elastic moduli between 0.5 and 10 GPa were used for the bottom rectangular cuboid to study the effect of different elastic moduli on nonuniform, mechanically graded specimens. The magnitude and von Mises stress distribution were determined for the different combinations of elastic moduli and Poisson's ratio.

Photoelasticity Tensile Testing

Photoelastic tensile testing was performed as previously described with minor modifications.[86] Specimens (2.2 cm × 12.7 cm × 0.6 cm) consisting of either uniform, nongraded QHM polymer samples (90 s UV, 120 s UV, or 300 s UV) or nonuniform, mechanically graded QHM polymer samples containing a single interface (90 s:120 s UV or 90 s:300 s UV) were fabricated. These dimensions were used to produce a wide QHM polymer sample to increase reproducibility by reducing the impact of a curved meniscus at the edges of the mold. While simplistic, a single interface was tested since gradients can be approximated by a continuous series of discrete intervals. Also, this setup facilitated ease of comparison with FEA simulations. Nonuniform, mechanically graded QHM polymer samples were fabricated by varying UV exposure to different halves of the same specimen. The average cross sectional area of QHM polymer samples was determined from three locations along the specimen gauge length using digital calipers. Photoelastic tensile testing was performed on a custom setup consisting of a Model 5944 test system (Instron Corp., Norwood MA) with the QHM polymer sample mounted in-between two left-handed, circularly polarized films (Edmund Optics Inc., Barrington, NJ). The films were oriented such that their polarizing axes were ≈90° relative to each other. The setup was backlit with a light box (Universal Medical Inc., Norwood, MA) and images of the photoelastic tensile testing were acquired using a Canon PowerShot S95 camera (Canon Inc., Melville, NY). Uniform, nongraded QHM polymer

Author Manuscript Author Manuscript Author Manuscript Author Manuscript

samples were uniaxially loaded at constant loads (0–500 N at intervals of 50 N) and used to construct a tensile-color interference chart (Figure S5, Supporting Information). This chart quantified stress distributions in nonuniform, mechanically graded QHM polymer samples with gradually graded (90 s:120 s UV) and steeply graded (90 s:300 s UV) interfaces. The 0 s UV QHM polymers were not used in these experiments as their high flexibility resulted in necking deformations at the interface of mechanically graded samples, posing difficulties in obtaining accurate stress and strain measurements due to the local decrease in cross sectional area.

Cell Culture

Multipotent mouse C2C12 myoblasts (ATTC, Manassas, VA) were grown in Dulbecco's modified Eagle's media (DMEM; Life Technologies, Carlsbad, CA), 10% fetal bovine serum (FBS; Life Technologies, Carlsbad, CA) and 1% PS. Cells were kept at 37 °C, 5% CO_2 in a humidified incubator. These cells were used as they serve as surrogate models of muscle-derived stem cells. Also, use of these cells minimizes the heterogeneous nature of primary cells, which often have varied proliferation rates depending on the source, methods of isolation, and characteristic marker profile. Hoechst staining (Anaspec, Fremont, CA) determined that cell cultures were free of mycoplasma contamination.

Degradation Studies

Degradation studies were performed on QHM polymer samples (circular discs ≈ 1 cm in diameter) under aqueous, alkaline, acidic, and oxidizing conditions. QHM polymer samples with a mass of ≈150 mg were weighed using a Mettler Toledo XS105 Dual Range weigh balance (Mettler Toledo International, Columbus, OH) and placed in 1.5 mL of the following solutions at 37 °C for 4 h, 1 week, 2 weeks, 4 weeks, or 8 weeks: (1) Hank's buffered salt solution (HBSS; Mediatech Inc, Manassas, VA), (2) 5 N sodium hydroxide, (3) 2 N hydrochloric acid (EMD Chemicals, Billerica, MA), and (4) 30% hydrogen peroxide (Thermo Fisher Scientific, Waltham, MA). No media change was performed. These conditions potentially approximated normal and chronic tissue microenvironments as well as potential foreign body reaction toward biomaterials. At each time point, wet weights were recorded, supernatants containing degradation products were collected and QHM polymer samples were processed to record dry weights. To obtain dried specimens, QHM polymer samples were washed in deionized water for 1 h followed by a series of graded ethanol washes (20% ethanol, 50% ethanol, 80% ethanol, and 100% ethanol; 10 min each) and placed under low vacuum in a desiccating chamber overnight. Degradation was determined by calculating the percentage of remaining mass at each time point. Swelling ratios at the 4 h time point were determined by calculating the mass difference between wet and dry weights and subsequently dividing the result by the dry weight.

Supernatants from the HBSS groups at 8 weeks were used for determining cell proliferation and differentiation in the presence of degradation products. HBSS supernatants from degradation studies were diluted in DMEM, 10% FBS and 1% PS media at a ratio of 1:9 to yield DMEM media containing degradation products. Dilution was necessary since QHM polymer samples were incubated in HBSS for an extended duration without media change (8 weeks) and a relatively low degradation solution to QHM polymer ratio (10:1) was used. A

Author Manuscript Author Manuscript Author Manuscript Author Manuscript

1:9 dilution of HBSS supernatant to DMEM media was chosen to maintain cell culture media at pH 7.4. C2C12 cells were seeded into 48 well plates at a density of 3.75×10^4 cells per cm^2 overnight. The following day (Day 0), media were changed to DMEM media containing degradation products. Cells were counted every 24 h using a Beckman Coulter Z2 Particle Counter. Cell differentiation was assessed using phase-contrast images acquired on an inverted Zeiss AxioObserver Z1 microscope equipped with an AxioCam MRm camera.

Suture Retention Testing

Suture retention testing was performed on 0 s UV QHM polymer and ADM samples. Samples were cut into rectangular specimens ≈20 mm (length) × 5 mm (width) × 1 mm (thickness). A suture hole was created 3 mm from the edge of the specimen using a Micromot 50/EF pen drill (Proxxon GmbH, Föhren, Germany) equipped with a 0.71 mm drill bit. Arthrex 4-0 FiberWire (Arthrex Inc., Naples, FL) was passed through the suture hole and secured in a 5 cm diameter loop using a simple, interrupted suture pattern. The suture loop was attached to a metal S-hook, which was subsequently mounted on a Model 5944 test system fitted with a 100 N load cell (Instron Corp., Norwood, MA). The other end of the sample was gripped between serrated jaws 5 mm from the sample edge. Samples were soaked in saline for 10 min prior to testing.

For suture retention testing, samples were preloaded to 0.1 N followed by loading between 0 and 7.5 N for 500 cycles at 0.5 Hz. The maximum value of this loading cycle was chosen to simulate one-third of the ultimate load for rat supraspinatus tendon.[71,72] Following cyclic testing, samples were pulled at a rate of 1 mm s^{-1} until failure. Suture migration was measured based on the change in suture position relative to the center of the suture hole. This migration was a result of suture hole stretching as well as suture tearing through the suture hole. Suture migration was monitored with a Model acA1600-20 g CCD camera (Basler Inc., Exton, PA). Suture retention testing and image data were synchronized and acquired at 20 Hz. Due to suture knot loosening and/or breakage, suture migration during load to failure was reported at 25 N, which was in excess of prior reports regarding the tensile strength of rat supraspinatus tendon.[71,72]

Rat Rotator Cuff Surgery

Tendon grafts containing recombinant human growth and differentiation Factor-7 (GDF-7; Sino Biological Inc., Beijing, China) for rat rotator cuff surgeries were prepared. 0 s UV QHM polymer or ADM were cut into square specimens ≈4.5 mm (length) × 4.5 mm (width) × 1 mm (thickness) and four suture holes were prefabricated using a Micromot 50/EF pen drill equipped with a 0.71 mm drill bit. GDF-7 was manually deposited onto tendon grafts using a micropipette (3 μL of a 1 mg mL^{-1} GDF-7 solution; 3 μg) the day before surgery. After deposition, samples were allowed to dry and then stored at 4 °C. Prior to implantation, GDF-7 containing tendon grafts were preloaded with 4-0 FiberWire sutures and immersed in phosphate buffered saline for 5 min to wash off unbound growth factor.

Rat rotator cuff surgeries were performed in accordance with the guidelines established by Stanford University's Administrative Panel on Laboratory Animal Care. Sprague Dawley

Author Manuscript Author Manuscript Author Manuscript Author Manuscript

rats (Charles River Laboratories, Wilmington, MA) between 20 and 23 weeks of age (500–675 g) were used in this study. All rats were maintained in the Stanford Animal Facility, with a 12:12 h light–dark cycle and free access to standard laboratory food and water. Rats were anesthetized by inhalation with isoflurane (4% for induction, 2% for maintenance, Abbott Laboratories, Chicago) and administered 2 mg kg^{-1} bupivacaine (Sigma Aldrich, St. Louis, MO) as a preoperative analgesic. Bilateral defects were created to facilitate paired analysis between 0 s UV QHM polymer and ADM tendon grafts. Under sterile conditions, a 3.5 cm skin incision was made and the rotator cuff tissues were exposed. Acromionectomy was performed and the supraspinatus tendon was detached at its insertion on the greater tuberosity. Following this, a Micromot 50/EF pen drill equipped with a 0.9 mm drill bit was used to create a suture hole in the humeral bone. Subsequently, the preloaded 4-0 FiberWire sutures of tendon grafts were passed through humeral bone and tendon to reapproximate tendon back to bone and augment the repair. Due to the small graft size and space constraints of the rat shoulder, simple interrupted suture patterns were used. Subsequently, the deltoid muscle and skin were reapproximated and closed with 3-0 poly glycolic acid and 3-0 nylon sutures, respectively. Rats were administered 25 mg kg^{-1} Cefazolin (Thermo Fisher Scientific, Waltham, MA) and 0.05 mg kg^{-1} Buprenorphine (Hospira Inc., Lake Forest, IL) as an antiinfective and postoperative analgesic, respectively. Rats were allowed to recover on a heating pad and returned to their cages without immobilization. At 8 weeks post-surgery, samples were harvested for biomechanical testing and histological analysis.

For biomechanical testing, samples comprising only of supraspinatus tendon, tendon graft, and humeral bone were obtained following rat shoulder dissection to remove extraneous soft tissues. The humerus was embedded in a hollow aluminum cylinder using polymethylmethacrylate. Testing was performed with the supraspinatus tendon loaded 90° relative to the long axis of the humerus using a custom set-up attached to a Model 5944 test system equipped with a 100 N load cell (Instron Corp., Norwood, MA) (Figure S7a, Supporting Information). Specimens were immersed in a phosphate buffered saline bath maintained at 37 °C throughout testing. The humerus was clamped with its long axis in the horizontal plane. The origin of the supraspinatus tendon was bonded between two pieces of sandpaper with cyanoacrylate glue. The sandpaper-tendon segment was then clamped vertically in a grip affixed to the testing machine (Figure S7b, Supporting Information). Digital calipers were used to determine the distance from the clamp to the tendon insertion (gauge length).

The test protocol was similar to that used in previous studies.[87–89] Specimens were preloaded to 0.2 N and preconditioned for five cycles to 5% strain at a rate of 1% strain/s. A stress relaxation test was then performed by ramping at 10% strain/s to 5% strain, maintaining 5% strain for 300 s, followed by 300 s of recovery. Specimens were then tested to tensile failure at a rate of 1% strain s^{-1}. Normalized tensile stiffness, ultimate load, and failure mode were determined for each specimen. Normalized tensile stiffness was defined as the slope of the load versus strain curve between 5% and 10% strain during load to failure tests. Ultimate load was the peak force achieved during the load to failure test.

For histological analysis, samples comprising of the rat shoulder joint with its respective implanted grafts were isolated for paraffin embedding, sectioning and staining. Samples

Author Manuscript Author Manuscript Author Manuscript Author Manuscript

were fixed in 4% paraformaldehyde (Sigma Aldrich, St. Louis, MO) for 1.5 d, decalcified in 10% ethylenediaminetetraacetic acid (EDTA), pH 7.4 (Sigma Aldrich, St. Louis, MO) for several weeks followed by a series of graded washes to allow for paraffin infiltration. This graded series included 1 h washes in 70% ethanol (1 wash at 25 °C), 85% ethanol (1 wash at 25 °C), 95% ethanol (2 washes at 25 °C), 100% ethanol (3 washes at 25 °C), 100% xylene (2 washes at 25 °C), and 100% paraffin (4 washes at 60 °C under vacuum) for an hour each. Paraffin-embedded samples were then sectioned (5–6 μm) using a Leica RM2235 microtome (Leica Biosystems, Wetzlar, Germany), deparaffinized and stained with either H&E or Masson's Trichrome. Tissue healing was assessed using brightfield images acquired on an inverted Olympus IX83 microscope equipped with a DP80 Double-CCD camera.

Statistical Analysis

All experiments were performed with at least 3 replicates per condition. Sample sizes were estimated to detect a group mean difference of 50% ± 1 to 2 standard deviations with a power $(1 - \beta)$ of 0.8 and $\alpha = 0.05$ (http://powerandsamplesize.com/Calculators/Compare-k-Means/1-Way-ANOVA-Pairwise). Quantitative data was presented as means ± standard error of mean (mean ± SEM) where appropriate. The Shapiro-Wilk test and the Levene test were used to determine whether data were normally distributed and contained equal variances among groups, respectively. To determine statistical significance for multiple comparisons, one-way analysis of variance followed by Tukey's honestly significant difference post hoc test was performed using SYSTAT 12 software (Systat Software Inc., Richmond, CA). For data that did not satisfy both normality and equal variance assumptions, Welch's analysis of variance followed by Games–Howell post hoc test was performed using IBM SPSS Statistics 23 software (SPSS Inc., Chicago, IL). This approach enables improved control of Type I errors and greater power under conditions of non-normality and heterogeneity of variance.[90] A p value ≤ 0.05 was considered statistically significant.

Data Availability

The authors declare that the data supporting the findings of this study are available within the paper and its Supporting Information files. Raw data are available from the corresponding authors upon reasonable request.

Supplementary Material

Refer to Web version on PubMed Central for supplementary material.

Acknowledgments

The authors would like to thank J. Tok from the Soft and Hybrid Materials Facility (Stanford University) for assistance with DSC analysis; I. Cheng (Stanford University), J. Helms (Stanford University), and D. Wan (Stanford University) for generous use of their equipment and facilities; L. Weiss (Carnegie Mellon University) for providing valuable input on growth factor delivery and manuscript edits. This work was supported by funding from the AO Foundation Startup Grant (S13-134K; D.F.E.K.), The Chinese University of Hong Kong (D.F.E.K. and D.W.), Department of Defense (W81XWH-10-1-0966; Y.P.Y.), NIH grants R01AR057837 (Y.P.Y.), R01DE021468 (Y.P.Y.), and U01AR069395 (Y.P.Y.), Stanford Biomedical Mini Seed Grant (Y.P.Y.), Stanford Coulter Seed Grant (Y.P.Y.), and Boswell Foundation (Y.P.Y.). D.F.E.K. designed the experiments, performed material fabrication, nuclear magnetic resonance spectroscopy, Fourier transformed infrared spectroscopy, mechanical testing, finite element analysis, photoelastic tensile testing, differential scanning calorimetry, degradation studies, suture retention testing, assisted in rat rotator cuff surgeries, biomechanical testing, analyzed the data, prepared the figures and

Author Manuscript Author Manuscript Author Manuscript Author Manuscript

wrote the manuscript. D.W. designed the experiments, performed material fabrication, finite element analysis, suture retention testing, specimen preparation for rat rotator cuff surgeries, histological staining, analyzed the data, prepared the figures, and wrote the manuscript. A.W.B. performed mechanical testing, finite element analysis, photoelastic tensile testing, suture retention testing, biomechanical testing and analyzed the data. E.T.H.W. performed finite element analysis, photoelastic tensile testing, and analyzed the data. X.Z. performed histological staining and analyzed the data. B.Y.Z. performed degradation studies. A.E.M.P. performed nuclear magnetic resonance spectroscopy, degradation studies, and provided valuable input on polymer fabrication. S.W.K. performed Fourier transformed infrared spectroscopy. J.K. performed rat rotator cuff surgeries. B.G. provided valuable input on growth factor delivery and assisted in writing the manuscript. Y.S. performed finite element analysis. D.N. performed photoelastic tensile testing, provided valuable input on mechanical testing studies, and assisted in writing the manuscript. M.S. provided valuable input on discussions concerning rotator cuff tears and wrote the manuscript. E.V.C. performed rat rotator cuff surgeries, provided valuable input on discussions concerning rotator cuff tears, and wrote the manuscript. P.C. provided valuable input on growth factor delivery and wrote the manuscript. Y.P.Y. designed the experiments, analyzed the data, and wrote the manuscript. All authors reviewed the manuscript.

References

1. Lu HH, Thomopoulos S. Annu Rev Biomed Eng. 2013; 15:201. [PubMed: 23642244]
2. Qu D, Mosher C, Boushell M, Lu H. Ann Biomed Eng. 2014; 43:697. [PubMed: 25465616]
3. Galatz LM, Gerstenfeld L, Heber-Katz E, Rodeo SA. J Orthop Res. 2015; 33:823. [PubMed: 25676657]
4. Longo UG, Franceschi F, Ruzzini L, Rabitti C, Morini S, Maffulli N, Denaro V. Am J Sports Med. 2008; 36:533. [PubMed: 18006676]
5. Gartsman, GM. Shoulder Arthroscopy. W. B. Saunders; Philadelphia, PA: 2009.
6. Cho NS, Rhee YG. Clin Orthop Surg. 2009; 1:96. [PubMed: 19885061]
7. Kim SJ, Kim SH, Lee SK, Seo JW, Chun YM. J Bone Jt Surg. 2013; 95:1482.
8. Fukubayashi T, Ikeda K. J Long-Term Eff Med Implants. 2000; 10:267. [PubMed: 11194610]
9. Walton JR, Bowman NK, Khatib Y, Linklater J, Murrell GA. J Bone Jt Surg. 2007; 89:786.
10. Andarawis-Puri N, Flatow EL, Soslowsky LJ. J Orthop Res. 2015; 33:780. [PubMed: 25764524]
11. Chaudhury S, Holland C, Thompson MS, Vollrath F, Carr AJ. J Shoulder Elbow Surg. 2011; 21:1168. [PubMed: 22079767]
12. Matsuhashi T, Hooke AW, Zhao KD, Goto A, Sperling JW, Steinmann SP, An KN. Clin Anat. 2014; 27:702. [PubMed: 24214830]
13. Belcher HJCR, Zic R. J Hand Surg, Br Eur. 2001; 26:159.
14. Derwin KA, Baker AR, Spragg RK, Leigh DR, Iannotti JP. J Bone Jt Surg. 2006; 88:2665.
15. Malcarney HL, Bonar F, Murrell GAC. Am J Sports Med. 2005; 33:907. [PubMed: 15827358]
16. Sclamberg SG, Tibone JE, Itamura JM, Kasraeian S. J Shoulder Elbow Surg. 2004; 13:538. [PubMed: 15383811]
17. Soler JA, Gidwani S, Curtis MJ. Acta Orthop Belg. 2007; 73:432. [PubMed: 17939470]
18. Alfredo Uquillas J, Kishore V, Akkus O. J the Mech Behav Biomed Mater. 2012; 15C:176.
19. Younesi M, Islam A, Kishore V, Anderson JM, Akkus O. Adv Funct Mater. 2014; 24:5762. [PubMed: 25750610]
20. Inui A, Kokubu T, Fujioka H, Nagura I, Sakata R, Nishimoto H, Kotera M, Nishino T, Kurosaka M. Sports Med, Arthrosc, Rehabil, Ther Technol. 2011; 3:29. [PubMed: 22136125]
21. Inui A, Kokubu T, Mifune Y, Sakata R, Nishimoto H, Nishida K, Akisue T, Kuroda R, Satake M, Kaneko H, Fujioka H. Arthroscopy. 2012; 28:1790. [PubMed: 23058811]
22. Liu W, Lipner J, Moran CH, Feng L, Li X, Thomopoulos S, Xia Y. Adv Mater. 2015; 27:2583. [PubMed: 25758008]
23. Makris EA, Responte DJ, Paschos NK, Hu JC, Athanasiou KA. Proc Natl Acad Sci USA. 2014; 111:E4832. [PubMed: 25349395]
24. McCarron JA, Milks RA, Chen X, Iannotti JP, Derwin KA. J Shoulder Elbow Surg. 2010; 19:688. [PubMed: 20413333]
25. Chin L, Calabro A, Walker E, Derwin KA. J Biomed Mater Res, Part A. 2012; 100:786.

Author Manuscript Author Manuscript Author Manuscript Author Manuscript

26. Spalazzi JP, Dagher E, Doty SB, Guo XE, Rodeo SA, Lu HH. Presented at Annual Int Conf Proc of the IEEE Engineering in Medicine and Biology Society, New York, USA. 2006
27. Spalazzi JP, Dagher E, Doty SB, Guo XE, Rodeo SA, Lu HH. J Biomed Mater Res, Part A. 2008; 86:1.
28. Spalazzi JP, Doty SB, Moffat KL, Levine WN, Lu HH. Tissue Eng. 2006; 12:3497. [PubMed: 17518686]
29. Caliari SR, Harley BA. Tissue Eng, Part A. 2013; 19
30. Caliari SR, Harley BAC. Biomaterials. 2011; 32:5330. [PubMed: 21550653]
31. Caliari SR, Harley BAC. Adv Healthcare Mater. 2014; 3:1086.
32. Xie J, Li X, Lipner J, Manning CN, Schwartz AG, Thomopoulos S, Xia Y. Nanoscale. 2010; 2:923. [PubMed: 20648290]
33. Xie J, Ma B, Michael PL, Shuler FD. Macromol Biosci. 2012; 12:1336. [PubMed: 22847852]
34. Li X, Xie J, Lipner J, Yuan X, Thomopoulos S, Xia Y. Nano Lett. 2009; 9:2763. [PubMed: 19537737]
35. Ramalingam M, Young MF, Thomas V, Sun L, Chow LC, Tison CK, Chatterjee K, Miles WC, Simon CG. J Biomater Appl. 2013; 27:695. [PubMed: 22286209]
36. Smith MJ, Cook JL, Kuroki K, Jayabalan PS, Cook CR, Pfeiffer FM, Waters NP. Arthroscopy. 2012; 28:169. [PubMed: 22137238]
37. Itoi E, Berglund LJ, Grabowski JJ, Schultz FM, Growney ES, Morrey BF, An KN. J Orthop Res. 1995; 13:578. [PubMed: 7674074]
38. Wall JC, Chatterji SK, Jeffery JW. Calcif Tissue Int. 1979; 27:105. [PubMed: 110411]
39. Yuehuei, A, Robert, D. Mechanical Testing of Bone and the Bone-Implant Interface. CRC Press; Boca Raton, FL: 1999.
40. Lichtwark GA, Wilson AM. J Biomech. 2007; 40:1768. [PubMed: 17101140]
41. Lichtwark GA, Wilson AM. J Theor Biol. 2008; 252:662. [PubMed: 18374362]
42. Barber FA. Arthroscopy. 2007; 23:316. [PubMed: 17349477]
43. Joo Han O, Byung Wook S, Tae-Yon R. Clin Shoulder Elbow. 2015; 18:254.
44. Bostman OM, Pihlajamaki HK. Clin Orthop Relat Res. 2000; 371:216.
45. Glueck D, Wilson TC, Johnson DL. Am J Sports Med. 2005; 33:742. [PubMed: 15722290]
46. Baleani M, Schrader S, Veronesi CA, Rotini R, Giardino R, Toni A. Clin Biomech. 2003; 18:721.
47. Cummins CA, Appleyard RC, Strickland S, Haen PS, Chen S, Murrell GA. Arthroscopy. 2005; 21:1236. [PubMed: 16226653]
48. Mercado-Pagan AE, Kang Y, Ker DF, Park S, Yao J, Bishop J, Yang Y. Eur Polym J. 2013; 49:3337. [PubMed: 24817764]
49. Silverstein, RM, Webster, FX, Kiemle, DJ. Spectrometric Identification of Organic Compounds. John Wiley & Sons; Hoboken, NJ: 2005.
50. Kim S, Kang Y, Mercado-Pagan AE, Maloney WJ, Yang Y. J Biomed Mater Res, Part B. 2014; 102:1393.
51. Ide J, Mochizuki Y, van Noort A, Ochi H, Sridharan S, Itoi E, Greiner S. Orthop J Sports Med. 2017; 5
52. Wolfman NM, Hattersley G, Cox K, Celeste AJ, Nelson R, Yamaji N, Dube JL, DiBlasio-Smith E, Nove J, Song JJ, Wozney JM, Rosen V. J Clin Invest. 1997; 100:321. [PubMed: 9218508]
53. Mather RC III, Koenig L, Acevedo D, Dall TM, Gallo P, Romeo A, Tongue J, Williams JG. J Bone Jt Surg. 2013; 95:1993.
54. Benjamin M, Ralphs JR. J Anat. 1998; 193:481. [PubMed: 10029181]
55. Benjamin M, Toumi H, Ralphs JR, Bydder G, Best TM, Milz S. J Anat. 2006; 208:471. [PubMed: 16637873]
56. Szycher, M. Szycher's Handbook of Polyurethanes. 2nd. CRC Press; Boca Raton, FL: 2012.
57. Bruin P, Meeuwsen EA, van Andel MV, Worst JG, Pennings AJ. Biomaterials. 1993; 14:1089. [PubMed: 7508760]
58. Wang H, Brown HR. Macromol Rapid Commun. 2004; 25:1095.

Author Manuscript Author Manuscript Author Manuscript Author Manuscript

59. Chandrashekar N, Slauterbeck J, Hashemi J. Knee. 2012; 19:65. [PubMed: 21216601]
60. Wren TA, Yerby SA, Beaupre GS, Carter DR. Clinical Biomech. 2001; 16:245.
61. Genin GM, Kent A, Birman V, Wopenka B, Pasteris JD, Marquez PJ, Thomopoulos S. Biophys J. 2009; 97:976. [PubMed: 19686644]
62. Liu Y, Birman V, Chen C, Thomopoulos S, Genin GM. J Eng Mater Technol. 2011; 133:011006. [PubMed: 21743758]
63. Rossetti L, Kuntz LA, Kunold E, Schock J, Muller KW, Grabmayr H, Stolberg-Stolberg J, Pfeiffer F, Sieber SA, Burgkart R, Bausch AR. Nat Mater. 2017; 16:664. [PubMed: 28250445]
64. Ker RF. J Exp Biol. 1981; 93:283. [PubMed: 7288354]
65. Nagasawa K, Noguchi M, Ikoma K, Kubo T. Clin Biomech. 2008; 23:832.
66. Deakin M, Stubbs D, Bruce W, Goldberg J, Gillies RM, Walsh WR. Arthroscopy. 2005; 21:1447. [PubMed: 16376233]
67. Cobaleda Aristizabal AF, Sanders EJ, Barber FA. Arthroscopy. 2014; 30:555. [PubMed: 24650833]
68. Fukuda H, Mikasa M. J Orthop Sci. 2007; 12:4. [PubMed: 17260111]
69. Schneider LA, Korber A, Grabbe S, Dissemond J. Arch Dermatol Res. 2007; 298:413. [PubMed: 17091276]
70. Anderson JM, Rodriguez A, Chang DT. Semin Immunol. 2008; 20:86. [PubMed: 18162407]
71. Beason DP, Connizzo BK, Dourte LM, Mauck RL, Soslowsky LJ, Steinberg DR, Bernstein J. J Shoulder Elbow Surg. 2012; 21:245. [PubMed: 22244068]
72. Ide J, Kikukawa K, Hirose J, Iyama K, Sakamoto H, Mizuta H. J Shoulder Elbow Surg. 2009; 18:288. [PubMed: 19058978]
73. Hsu JE, Reuther KE, Sarver JJ, Lee CS, Thomas SJ, Glaser DL, Soslowsky LJ. J Orthop Res. 2011; 29:1028. [PubMed: 21308755]
74. Steinhaus ME, Makhni EC, Cole BJ, Romeo AA, Verma NN. Arthroscopy. 2016; 32:1676. [PubMed: 27157657]
75. Ker ED, Chu B, Phillippi JA, Gharaibeh B, Huard J, Weiss LE, Campbell PG. Biomaterials. 2011; 32:3413. [PubMed: 21316755]
76. Ker ED, Nain AS, Weiss LE, Wang J, Suhan J, Amon CH, Campbell PG. Biomaterials. 2011; 32:8097. [PubMed: 21820736]
77. Lamplot JD, Angeline M, Angeles J, Beederman M, Wagner E, Rastegar F, Scott B, Skjong C, Mass D, Kang R, Ho S, Shi LL. Am J Sports Med. 2014; 42:2877. [PubMed: 25193888]
78. Lee JY, Zhou Z, Taub PJ, Ramcharan M, Li Y, Akinbiyi T, Maharam ER, Leong DJ, Laudier DM, Ruike T, Torina PJ, Zaidi M, Majeska RJ, Schaffler MB, Flatow EL, Sun HB. PloS One. 2011; 6:e17531. [PubMed: 21412429]
79. Chen X, Yin Z, Chen J-L, Liu H-H, Shen W-L, Fang Z, Zhu T, Ji J, Ouyang H-W, Zou X-H. Tissue Eng, Part A. 2013; 20:1583.
80. Gulotta LV, Kovacevic D, Packer JD, Deng XH, Rodeo SA. Am J Sports Med. 2011; 39:1282. [PubMed: 21335341]
81. Hoffmann A, Pelled G, Turgeman G, Eberle P, Zilberman Y, Shinar H, Keinan-Adamsky K, Winkel A, Shahab S, Navon G, Gross G, Gazit D. J Clin Invest. 2006; 116:940. [PubMed: 16585960]
82. Otabe K, Nakahara H, Hasegawa A, Matsukawa T, Ayabe F, Onizuka N, Inui M, Takada S, Ito Y, Sekiya I, Muneta T, Lotz M, Asahara H. J Orthop Res. 2014; 33:1. [PubMed: 25312837]
83. Phillips JE, Garcia AJ. Methods Mol Biol. 2008; 433:333. [PubMed: 18679633]
84. Meyer D, Hoppeler H, Gerber C. J Bone Jt Surg, Br. 2008; 90-B:293.
85. Hersche O, Gerber C. J Shoulder Elbow Surg. 1998; 7:393. [PubMed: 9752650]
86. Murphy EB. J Mater Chem. 2011; 21:1438.
87. Baumgarten KM, Oliver HA, Foley J, Chen DG, Autenried P, Duan S, Heiser P. J Bone Jt Surg. 2013; 95:783.
88. Galatz LM, Charlton N, Das R, Kim HM, Havlioglu N, Thomopoulos S. J Shoulder Elbow Surg. 2009; 18:669. [PubMed: 19427237]
89. Harada Y, Mifune Y, Inui A, Sakata R, Muto T, Takase F, Ueda Y, Kataoka T, Kokubu T, Kuroda R, Kurosaka M. J Orthop Res. 2017; 35:289. [PubMed: 27171575]

Author Manuscript Author Manuscript Author Manuscript Author Manuscript

90. Tomarken AJ, Serlin RC. Psychol Bull. 1986; 99:90.

Author Manuscript Author Manuscript Author Manuscript Author Manuscript

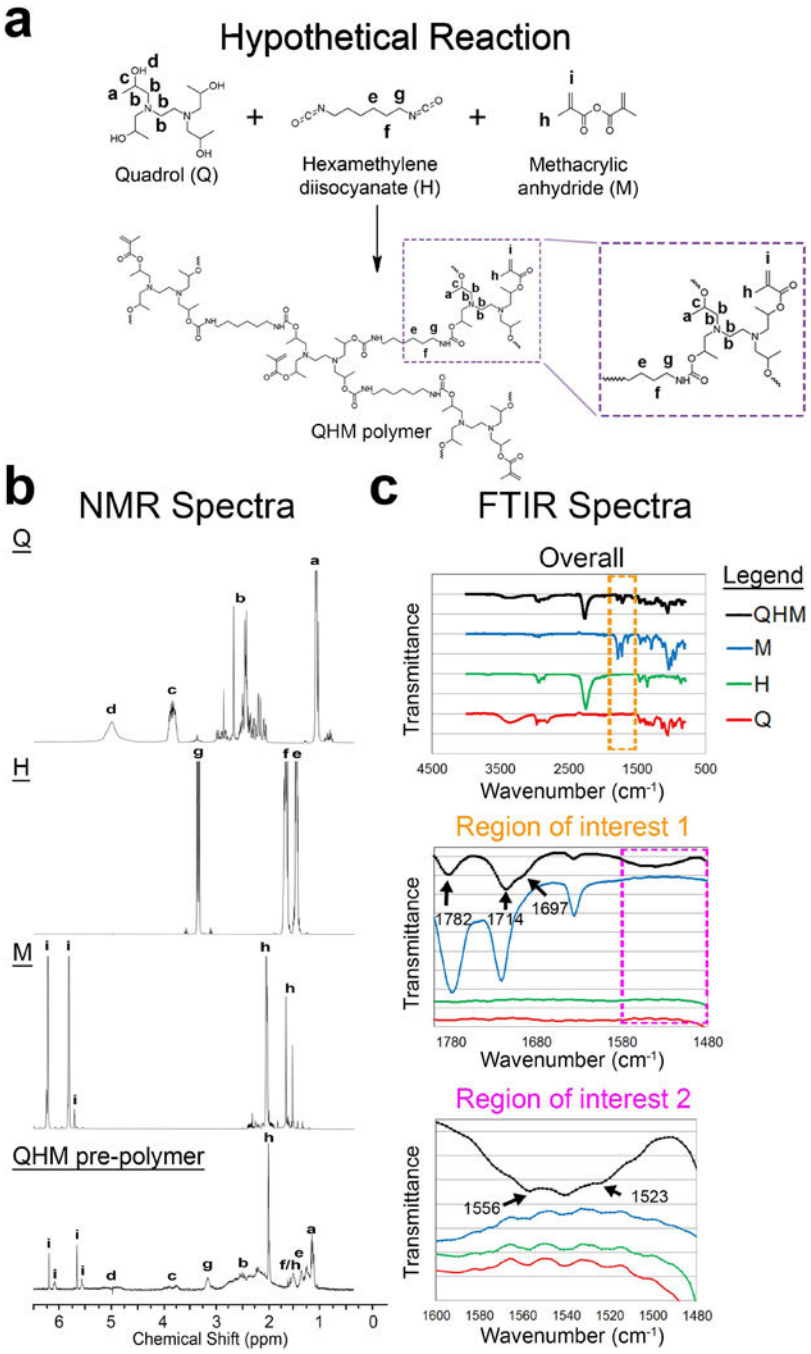

Figure 1.

Synthesis of QHM polymer. a) Hypothetical reaction scheme for QHM polymer synthesis. b) ^{1}H-NMR spectra of individual QHM polymer components and QHM prepolymer. ^{1}H-NMR peaks indicated by letters were assigned to their respective protons in the chemical structures. c) FTIR-ATR spectra of individual QHM polymer components and QHM prepolymer. Regions of interest 1 and 2 are indicated by orange and magenta dashed boxes, respectively.

Author Manuscript Author Manuscript Author Manuscript Author Manuscript

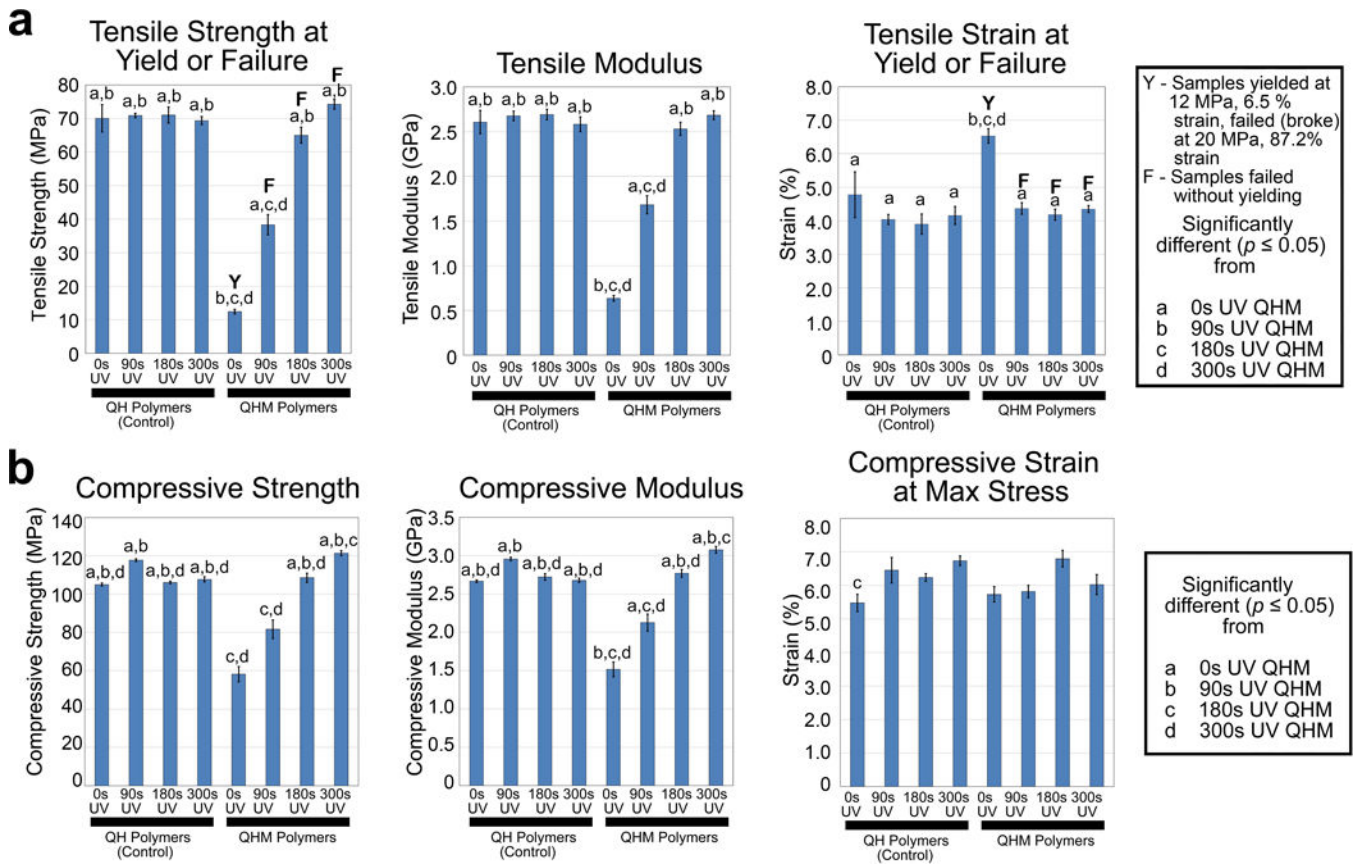

Figure 2.

Tensile and compressive properties of QHM polymers. a) Uniaxial tensile testing of QHM polymers ($n = 6$; 3 independent experiments). *Y* indicates that sample yield value was reported whereas *F* indicates that sample failure value was reported. b) Uniaxial compressive testing of QHM polymers ($n = 6$; 3 independent experiments). Statistical significance ($p \leq 0.05$) as indicated. Error bars indicate standard error of mean.

Author Manuscript Author Manuscript Author Manuscript Author Manuscript

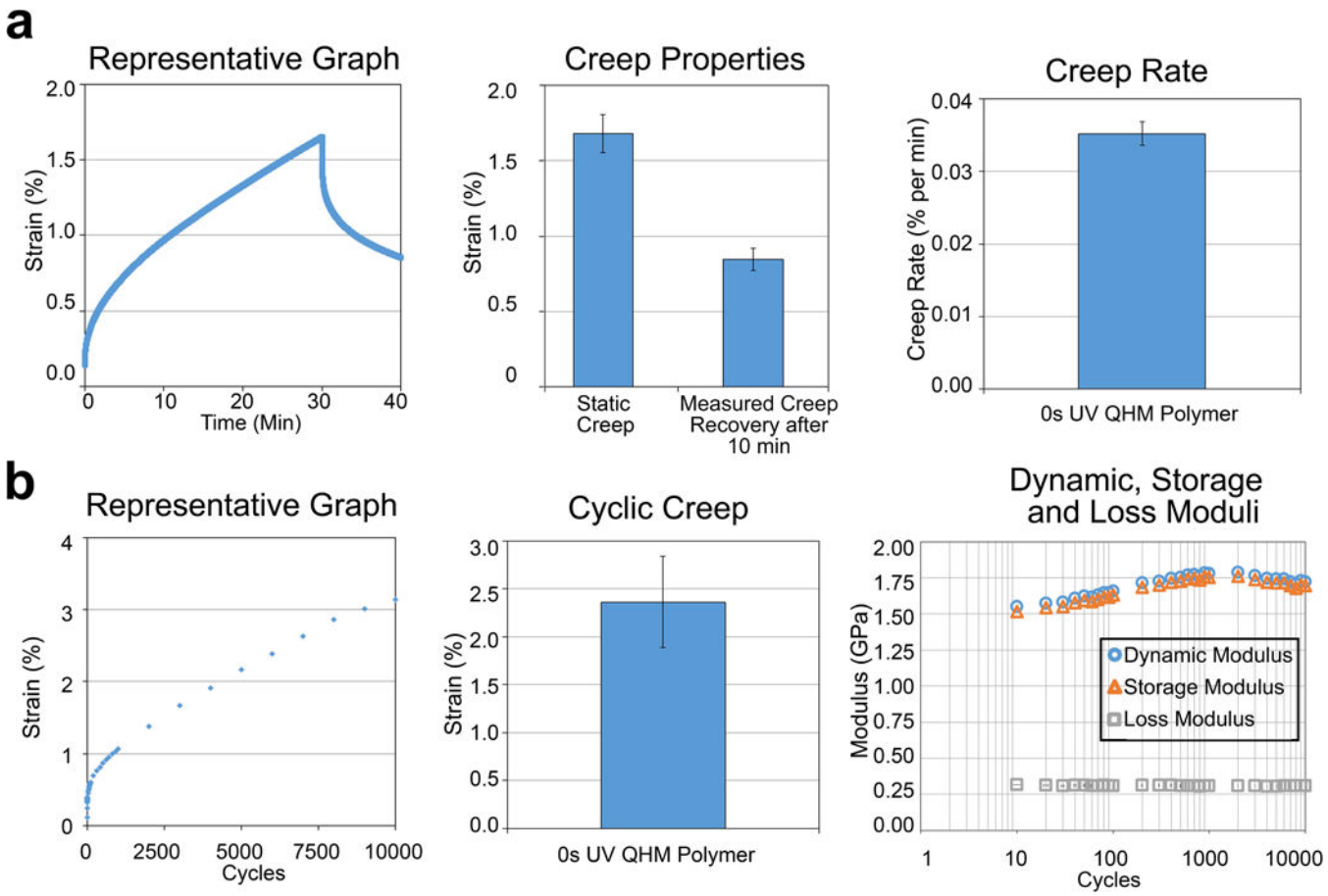

Figure 3.

Static and cyclic tensile properties of 0 s UV QHM polymer. a) Static creep tensile testing (3 MPa) of 0 s UV QHM polymer ($n = 3$). b) Cyclic tensile testing (10 000 cycles from 0.2 to 3 MPa at 1 Hz) of 0 s UV QHM polymer ($n = 3$). Error bars indicate standard error of mean.

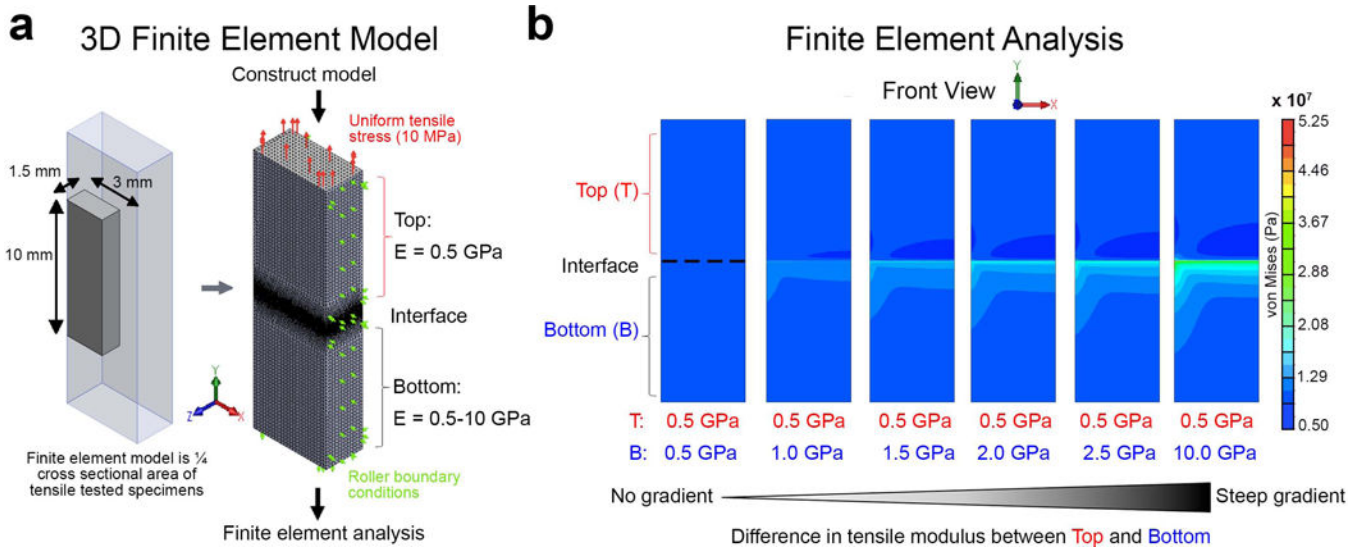

Figure 4.

Finite element analysis of gradually- and steeply graded specimens. a) 3D finite element model used in simulations. Finite element analysis of uniform or mechanically graded quarter models with gradually- and steeply graded interfaces subjected to 10 MPa tensile stress. A Poisson's ratio of 0.3 was used for top and bottom halves of each model. b) The effect of different stiffness gradients on stress concentrations in finite element simulations. Peak values of concentrated stress not presented in color plot.

Author Manuscript Author Manuscript Author Manuscript Author Manuscript

Author Manuscript Author Manuscript Author Manuscript Author Manuscript

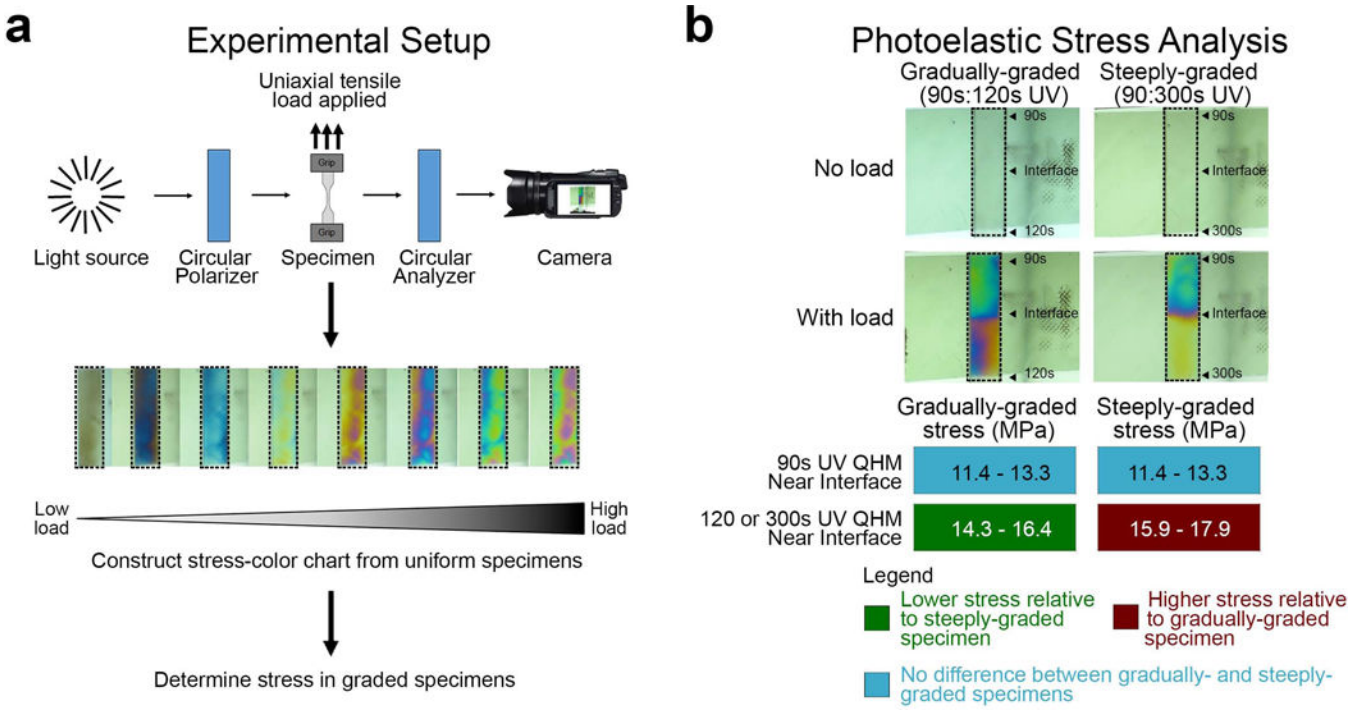

Figure 5.

Photoelastic stress analysis of gradually- and steeply graded QHM polymers. a) Experimental setup of photoelastic stress analysis. b) The effect of different stiffness gradients on stress concentrations in QHM polymers. Representative images of photoelastic tensile analysis for mechanically graded specimens with gradually- and steeply graded interfaces from 3 independent experiments. Dashed boxes indicate photoelastic specimens.

Author Manuscript Author Manuscript Author Manuscript Author Manuscript

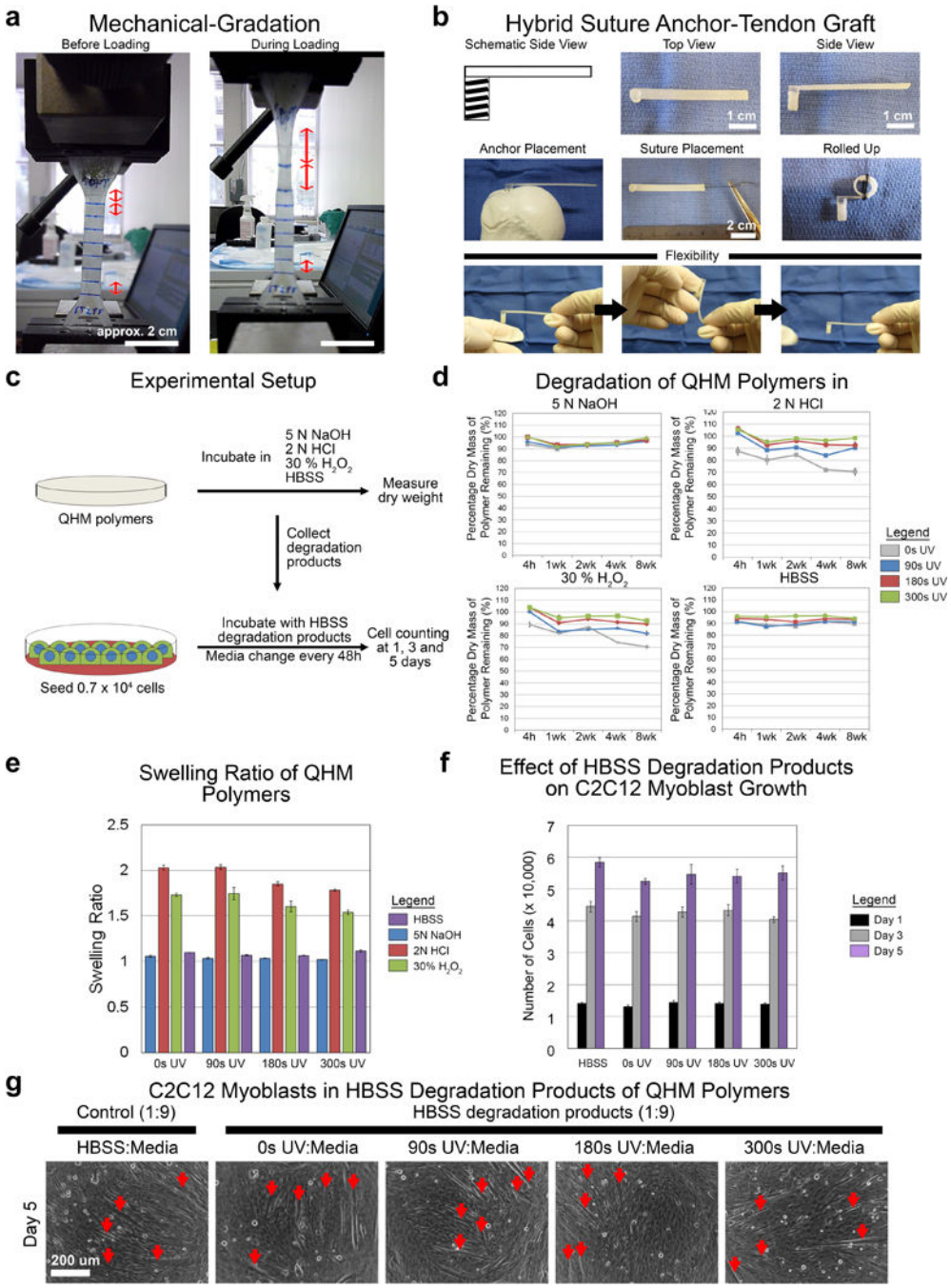

Figure 6.

Mechanically graded, hybrid suture anchor-tendon graft and degradation of QHM polymers. a) Representative images of mechanically graded QHM polymer. b) Representative images of mechanically graded QHM polymer fabricated as a hybrid suture anchor-tendon graft. c) Experimental setup of degradation studies. d) Degradation of QHM polymers under alkaline (5 N NaOH), acidic (2 N HCl), oxidizing (30% H_2O_2), and aqueous (HBSS) conditions at 37 °C over 8 weeks ($n = 6$; 1 independent experiment). e) Swelling ratio of QHM polymers under alkaline (5 N NaOH), acidic (2 N HCl), oxidizing (30% H_2O_2), and aqueous (HBSS)

Author Manuscript Author Manuscript Author Manuscript Author Manuscript

conditions after 4 h at 37 °C (n = 6; 1 independent experiment). f) Proliferation of C2C12 cells in 8-week HBSS degradation products (diluted 1:9 in media) of various QHM polymers during 5 d of culture (n = 6; 2 independent experiments). g) Spontaneous differentiation of C2C12 cells into myotubes (red arrows) after 5 d of proliferation in 8-week HBSS degradation products (diluted 1:9 in media). Scale bars as indicated. Error bars indicate standard error of mean.

Author Manuscript Author Manuscript Author Manuscript Author Manuscript

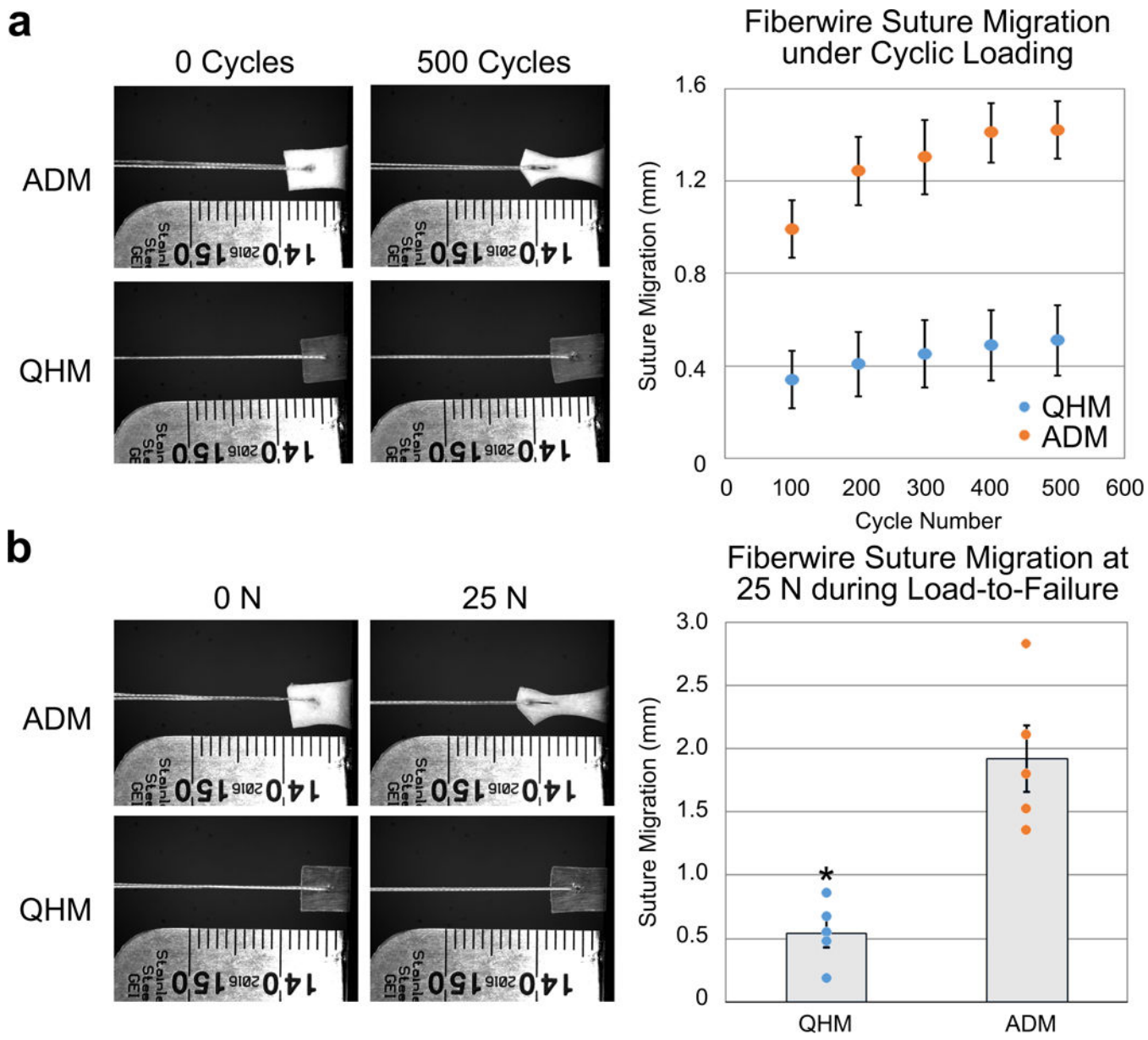

Figure 7.

Suture retention of 0 s UV QHM polymer and ADM. a) Cyclic suture retention testing (500 cycles from 0 to 7.5 N at 0.5 Hz) of 0 s UV QHM polymer and ADM ($n = 5$). b) 0 s UV QHM polymer and ADM were loaded to failure following cyclic suture retention testing ($n = 5$). Error bars indicate standard error of mean. *: Statistical significance ($p \leq 0.05$) relative to ADM.

Author Manuscript Author Manuscript Author Manuscript Author Manuscript

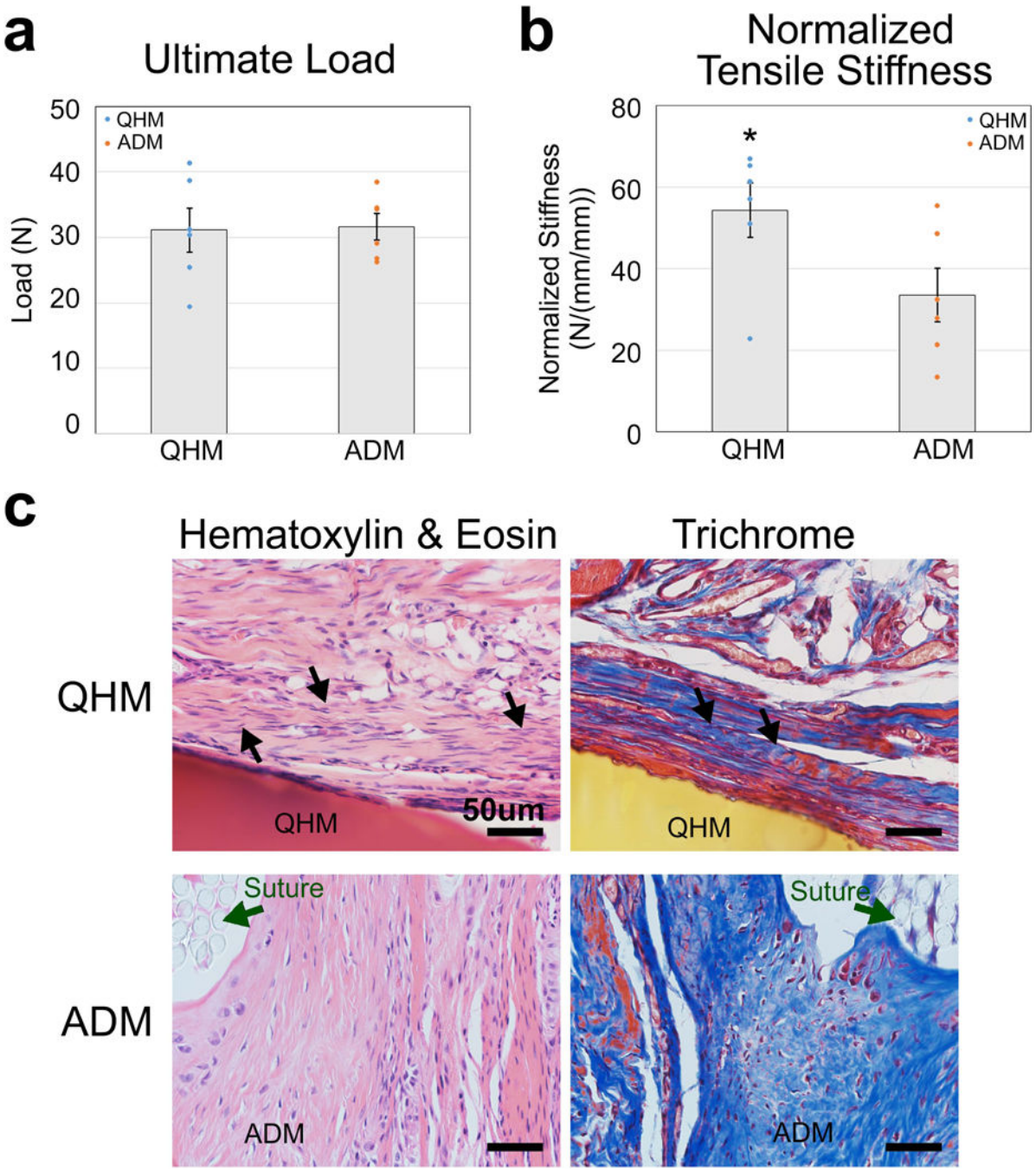

Figure 8.

Biomechanical properties and histology of rat supraspinatus muscle-tendon-bone unit 8 weeks after tendon resection and graft-augmented repair. a) Ultimate load of rat supraspinatus muscle-tendon-bone unit 8 weeks after 0 s UV QHM polymer- or ADM-mediated repair (n = 6, 3 independent experiments). b) Normalized tensile stiffness of rat supraspinatus muscle-tendon-bone unit 8 weeks after 0 s UV QHM polymer- or ADM-mediated repair. Stiffness is normalized by taking the slope of the load versus strain (specimen displacement/original length) for equal area (n = 6, 3 independent experiments).

Author Manuscript Author Manuscript Author Manuscript Author Manuscript

c) Hematoxylin and eosin (H&E) and trichrome staining of rat bone-tendon tissue 8 weeks after 0 s UV QHM polymer- or ADM-mediated repair. In H&E images, cell nuclei stained purple whereas cell cytoplasm and extracellular matrix stained pink. 0 s UV QHM polymer and ADM stained red and pink, respectively. In Trichrome images, cell nuclei stained black, cell cytoplasm as well as muscle fibers stained red/pink whereas collagen fibers stained blue. 0 s UV QHM polymer and ADM stained yellow and blue, respectively. Dark green arrows indicate sutures (circular light gray structures). Black arrows indicate aligned and wavy extracellular fibers embedded with elongated tendon-like cells ($n = 3$, 1 independent experiment). Scale bars 50 μm. Error bars indicate standard error of mean. *: Statistical significance ($p \leq 0.05$) relative to ADM.